



Directed evolution of an efficient and thermostable PET depolymerase

Elizabeth L. Bell¹, Ross Smithson¹, Siobhan Kilbride², Jake Foster¹, Florence J. Hardy¹, Saranarayanan Ramachandran², Aleksander A. Tedstone³, Sarah J. Haigh¹, Arthur A. Garforth¹, Philip J. R. Day⁴, Colin Levy¹, Michael P. Shaver¹ and Anthony P. Green¹✉

The recent discovery of *IsPETase*, a hydrolytic enzyme that can deconstruct poly(ethylene terephthalate) (PET), has sparked great interest in biocatalytic approaches to recycle plastics. Realization of commercial use will require the development of robust engineered enzymes that meet the demands of industrial processes. Although rationally engineered PETases have been described, enzymes that have been experimentally optimized via directed evolution have not previously been reported. Here, we describe an automated, high-throughput directed evolution platform for engineering polymer degrading enzymes. Applying catalytic activity at elevated temperatures as a primary selection pressure, a thermostable *IsPETase* variant (HotPETase, $T_m = 82.5^\circ\text{C}$) was engineered that can operate at the glass transition temperature of PET. HotPETase can depolymerize semicrystalline PET more rapidly than previously reported PETases and can selectively deconstruct the PET component of a laminated multmaterial. Structural analysis of HotPETase reveals interesting features that have emerged to improve thermo-tolerance and catalytic performance. Our study establishes laboratory evolution as a platform for engineering useful plastic degrading enzymes.

Poly(ethylene terephthalate) (PET) is among the most abundantly produced synthetic polymers. Demand for this material has grown substantially due to a heightened global appetite for convenient single-use containers^{1,2}, with an estimated 1 million PET bottles being produced every minute³. Although mechanical recycling methods are available for PET, recycling rates remain low due to difficulties in collecting and sorting mixed postconsumer waste streams^{4,5}, and declining polymer properties after repeated processing cycles⁶. In light of these challenges, depolymerization of PET into its component monomers has attracted interest as a means of circularizing the PET life cycle^{7,8}. This can be achieved using chemical recycling techniques, including solvolysis methods such as hydrolysis and glycolysis^{9,10}. More recently, enzymatic depolymerizations have emerged as a potentially attractive alternative^{7,8}. Techno-economic analysis and life-cycle assessments predict that biocatalysis can offer a cost-effective and energy efficient approach to PET recycling. Furthermore, enzymatic recycling could also facilitate selective depolymerizations of complex mixed feedstock waste streams that are particularly challenging to recycle effectively.

For enzymatic PET recycling to be feasible, suitable biocatalysts must first be discovered and then engineered to tailor their properties for target applications. Unfortunately, while microorganisms are extremely well-equipped to deconstruct biological polymers such as proteins, DNA and carbohydrates, they are generally not well-adapted to achieve efficient depolymerization of synthetic polymers¹¹. Nevertheless, some cutinases have been shown to have promiscuous PET degradation abilities^{12–15}. These enzymes typically display poor activity towards PET materials with high crystallinities, akin to those commonly found in postconsumer waste. To function effectively, even engineered cutinases require the extensive

preprocessing of PET substrates to amorphize the material¹⁶, a process that compromises the economic and environmental sustainability of biocatalytic plastic recycling approaches¹⁷.

The recent discovery of an organism, *Ideonella sakaiensis*, with the ability to use PET as a carbon source¹⁸, revealed a naturally evolved, PET-hydrolysing enzyme (*IsPETase*^{WT}) that has an enhanced ability to depolymerize more crystalline forms of PET^{18,19}. There are interesting structural differences between *IsPETase* and homologous cutinases, which are thought to be linked to this improved activity¹⁹, including a conformationally flexible Trp185 that has been proposed to aid polymer binding^{20,21}. The unique catalytic properties of *IsPETase* make it an attractive candidate as a biocatalyst for PET recycling. Unfortunately, the wild-type enzyme suffers from low thermostability¹⁸, meaning that biotransformations must be run at ambient temperatures far below the glass transition temperature (T_g) of PET (T_g of approximately 60–70 °C), which compromises polymer deconstruction rates^{22,23}.

In an effort to address these limitations, improvements in PETase stability have been achieved using a variety of rational engineering approaches^{19,24–27}. In contrast, experimental optimization of *IsPETase* using directed evolution, which typically offers a more comprehensive approach to enzyme engineering^{28,29}, remains under-explored, probably due to the lack of suitable protocols for monitoring the deconstruction of insoluble plastics with sufficient throughput³⁰. Here we establish an automated, high-throughput directed evolution platform for engineering plastic deconstructing enzymes and showcase its use by engineering a thermostable variant of *IsPETase* that can operate at the glass transition temperature of PET. This engineered biocatalyst can efficiently depolymerize semicrystalline PET and can selectively deconstruct real-world laminated packaging materials.

¹Manchester Institute of Biotechnology, University of Manchester, Manchester, UK. ²Department of Materials, University of Manchester, Manchester, UK.

³Department of Chemical Engineering and Analytical Science, University of Manchester, Manchester, UK. ⁴Division of Evolution and Genomic Sciences, Faculty of Biology, Medicine and Health, University of Manchester, Manchester, UK. ✉e-mail: anthony.green@manchester.ac.uk

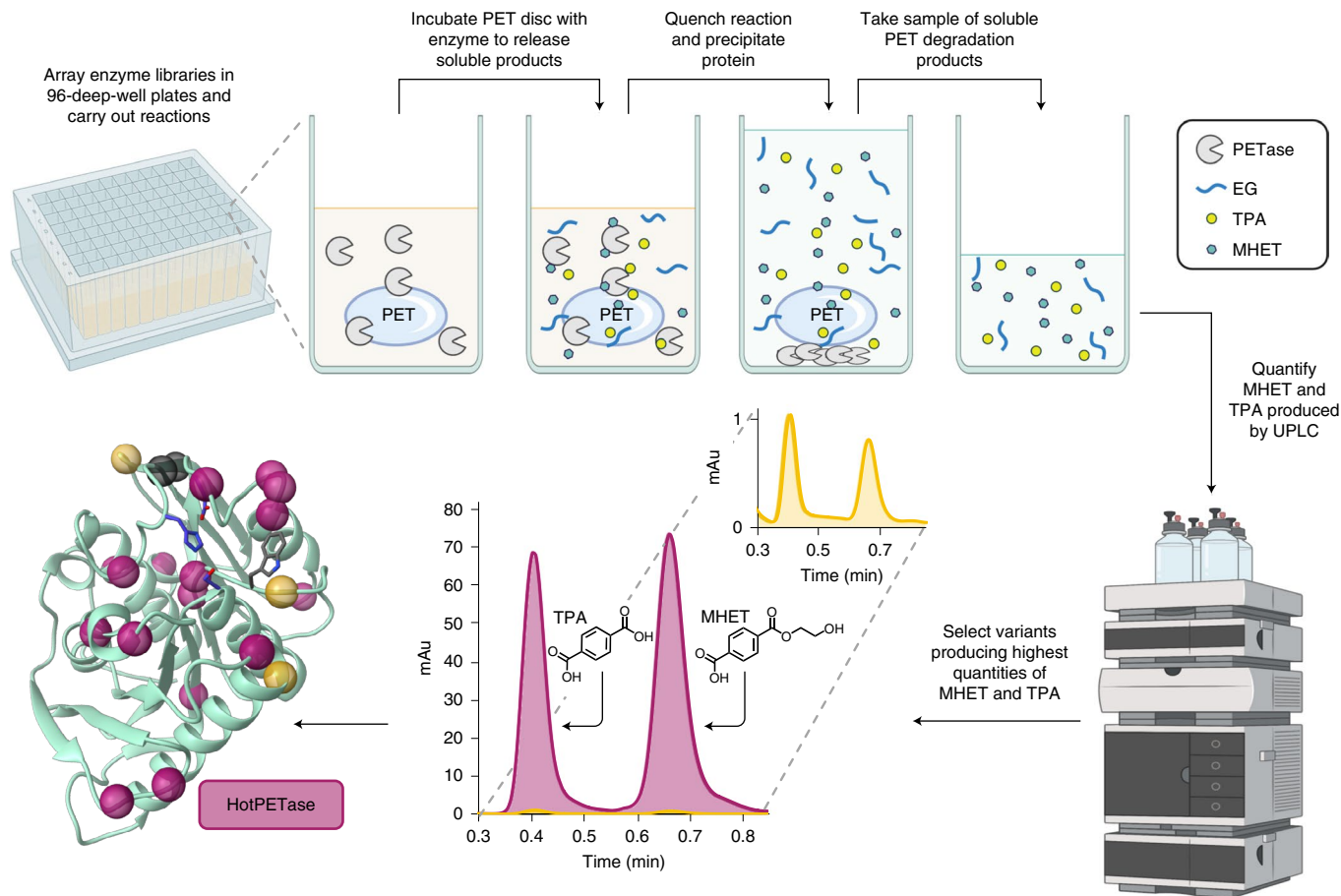


Fig. 1 | Workflow for the directed evolution of a PET depolymerase. Depiction of the laboratory evolution workflow for a single well in a 96-deep-well plate. Enzymatic PET depolymerizations mainly produce MHET, TPA and ethylene glycol (EG). The example UPLC trace demonstrates the MHET and TPA produced following a 5 h PET degradation reaction of semicrystalline PET powder (cryPET), with absorbance on the y axis in milli-absorbance units (mAu) and retention time on the x axis in minutes (min). Reactions were carried out at 70 °C, with both the best variant following evolution, HotPETase (pink), and the starting protein *IsPETase*^{TS} (yellow) using 0.4% cryPET substrate loading (4 g l⁻¹) and 0.29 mg g⁻¹ enzyme loading (0.04 μM). The crystal structure shows the 21 amino acid positions mutated from *IsPETase*^{WT}: three positions mutated in the starting protein *IsPETase*^{TS} (yellow spheres), 16 installed through evolution (pink spheres) and a rationally installed disulfide bridge (black spheres). The catalytic triad and W185 are shown with a ball and stick representation in blue and grey, respectively.

Results

Directed evolution of a thermostable PETase. We selected a rationally designed, thermostabilized variant of *IsPETase* containing three mutations, S121E, D186H, R280A (*IsPETase*^{TS}, melting temperature (T_m) of 56.8 °C),²⁴ as a starting point for engineering. Consistent with previous reports, *IsPETase*^{TS} displays superior PET degradation activity compared to the wild-type enzyme at 40 °C; however, this activity decreases dramatically at more elevated temperatures (Supplementary Fig. 1).

Our first objective was to develop a high-throughput screening workflow to underpin the directed evolution study. To this end, individual enzyme variants were evaluated as crude cell lysates arrayed in 96-deep-well plates, using amorphous PET film (amoPET, 6.7% crystallinity, sourced from Goodfellow as a preform sheet) as the reaction substrate. The amoPET substrate allowed us to prepare uniform 6 mm diameter discs that could be easily placed into individual wells to allow fair comparison of variant activity (Fig. 1). We found that the addition of our standard chemical cell lysis reagents, lysozyme and polymyxin B, resulted in the production of a lysate with substantially reduced activity (Supplementary Fig. 2), hence, we developed a method for 96-well plate cell lysis using the commercial reagent, BugBuster. The accumulation of mono(2-hydroxyethyl) terephthalate (MHET) and terephthalic acid (TPA) in the reaction

supernatant was monitored by ultra performance liquid chromatography (UPLC); these two products result from the partial and complete hydrolysis of the PET backbone, respectively, and are the known major products of *IsPETase*-mediated depolymerizations^{18,31}. Using the UPLC method developed here, the MHET and TPA produced by a single degradation reaction can be analysed in under 2 minutes (Supplementary Fig. 2). Using our integrated, automated system, over 2,000 enzyme variants can be assessed for plastic deconstruction activity in around 2 days.

The evolutionary strategy comprised sequential rounds of saturation mutagenesis, using degenerate NNK codons to individually randomize between 24–30 residue positions per cycle. In total, 106 of the 264 residues present in *IsPETase* were targeted for mutation throughout evolution. Residues were selected for randomization on the basis of a number of considerations, including their identification by online protein stability-enhancing tools, visual inspection of the protein crystal structure or previous reports of their involvement in substrate binding or thermostability (Supplementary Table 1). In each round of evolution, around the top 3% of hits were assessed as purified enzymes. Beneficial mutations found were then combined by DNA shuffling, and the resulting variants assayed as purified proteins to identify the most active sequence, which was then used as a template for the next round of evolution. Between

rounds 2 and 3, an additional disulfide bridge (N233C, S282C) was rationally generated in the protein, following reports that the inclusion of this structural feature increased protein stability in homologous, promiscuous PET-degrading cutinases^{16,32}, leading to a 5.5 °C increase in T_m (Extended Data Fig. 1 and Supplementary Fig. 3).

To simultaneously improve both thermostability and activity, the evolutionary pressures applied were gradually changed across rounds by raising both the reaction temperature and extending the reaction time. For rounds 1–4, the primary focus was on improved catalysis at elevated temperatures. Cell lysates were pre-incubated at sequentially higher temperatures (from 55–75 °C) for 1 h, before conducting PET depolymerization reactions for 3 h. The reaction temperature also increased from 55–70 °C during these rounds (Supplementary Table 1). Once a satisfactory level of thermostability was achieved, additional selection pressures of catalyst longevity and activity on more crystalline material were added. To this end, reactions in rounds 5 and 6 were conducted at 70 °C, with reaction times of 5 and 7 h, respectively, initially using amoPET as the substrate. The top 3% of clones identified during rounds 5 and 6 were then screened as purified enzymes against a commercially available semicrystalline PET powder (cryPET, 29.8% crystallinity, sourced from Goodfellow) that has a crystallinity level more reminiscent of material dominant in postconsumer waste streams^{33,34}.

The most thermostable and active variant to emerge following six rounds of evolution, HotPETase, contains 21 mutations compared to *Is*PETase^{WT}: three from the starting protein template *Is*PETase^{TS}, two from the rational insertion of an additional disulfide bridge and a further 16 found through directed evolution (Fig. 1 and Extended Data Fig. 1). HotPETase has a melting temperature of 82.5 °C, the highest T_m recorded so far of an active *Is*PETase derivative. This elevated thermostability means that the enzyme can be incubated before reaction at 75 °C for 90 min with only a 6% loss of activity over 24 h (Supplementary Fig. 4). Enzyme pre-incubation at 80 °C for 90 min resulted in a more substantial 35% reduction in activity. Assessment of variants along the evolutionary trajectory demonstrated that evolution led to progressive improvements in both thermostability and activity in cryPET deconstruction assays performed at 60 °C (Fig. 2a and Supplementary Fig. 3). While *Is*PETase^{WT} and *Is*PETase^{TS} have minimal activity at 60 °C, HotPETase operated well under these conditions.

Biochemical characterization. We next determined the activity of HotPETase across a range of temperatures by monitoring the release of MHET and TPA over time (Fig. 2b). For comparison, analogous experiments were performed using the starting template, *Is*PETase^{TS}, and the engineered thermostable cutinase LCC^{ICCG} (ref. ¹⁶). Comparisons between LCC^{ICCG} and *Is*PETase variants were carried out under the optimal buffer conditions for each individual protein^{16,18}, using cryPET powder as the substrate (Supplementary Fig. 5). At 40 °C, slightly improved initial reaction rates were achieved by HotPETase versus *Is*PETase^{TS} (Fig. 2b), demonstrating that the evolution of thermostability has not compromised activity at ambient temperatures. While the activity of *Is*PETase^{TS} was severely compromised at higher temperatures, the rate of PET hydrolysis by HotPETase is substantially improved by operating at temperatures approaching the reported T_g of PET in aqueous solutions (around 60–65 °C)¹⁴. At 65 °C, each mole of HotPETase releases 2.7×10^4 M of monomers in 1 hour, a time-course over which reaction progression is linear. At the same temperature LCC^{ICCG} produced 5.7×10^3 moles of monomer product in the same time frame, highlighting the superior catalytic activity of this engineered *Is*PETase. For both HotPETase and LCC^{ICCG}, the reaction rates were slightly reduced at 70 versus 65 °C.

Comparison of reactions with HotPETase and *Is*PETase^{TS} at 40 °C show that evolution has afforded a more robust catalyst with increased longevity (Fig. 2c and Extended Data Fig. 2). For

*Is*PETase^{TS}, soluble product formation essentially ceases after 8 h. In contrast, for reactions with HotPETase, monomeric products continue to accumulate for more than 48 h. Consistent with previous studies²⁶, the reaction profile is non-linear with faster initial phase for roughly 8 h, followed by a slower phase from 8–48 h. Similar, but more pronounced, non-linear reaction profiles are observed at elevated temperatures (from 60–70 °C, Extended Data Fig. 2). The time-course of reactions with HotPETase at 65 °C demonstrate that product accumulation rises rapidly for the first of 3 h of reaction (1.51 mM of MHET + TPA), but then slows substantially after this time, producing 1.61 mM of soluble monomers over 48 h (Fig. 2d). As a result, while PET depolymerization with HotPETase is substantially faster at 65 °C, the extent of depolymerization at longer time frames is greater at 40 °C (Fig. 2c,d).

Product accumulation over time is also non-linear for LCC^{ICCG} in reactions at 65 °C, with 0.68 and 1.78 mM of monomers produced over 5 and 48 h, respectively (Extended Data Fig. 3). It is interesting to note that HotPETase operating at 40 °C deconstructs cryPET more efficiently than LCC^{ICCG} at 65 °C, both with respect to initial rate and extent of depolymerization over 48 h. HotPETase also depolymerizes amoPET discs (used for library screening) more effectively than LCC^{ICCG} across a range of temperatures from 40 to 65 °C (Supplementary Fig. 6). At 70 °C, although HotPETase produces more soluble monomers than LCC^{ICCG} over 3 h, at this temperature over 24 h, LCC^{ICCG} is a more effective depolymerase of amoPET due to its enhanced longevity.

To understand the origins of the non-linear reaction profiles of HotPETase, particularly at elevated temperatures, we conducted experiments to supply additional enzyme or substrate once reaction progression had ceased. Addition of fresh HotPETase, following cryPET depolymerization for 24 h at 60 °C, leads to similar product accumulation versus time trends as observed at the outset of the reaction (Extended Data Fig. 4). In contrast, addition of fresh PET substrate does not give rise to any additional soluble products. These observations suggest that reactions stall due to catalyst deactivation, not as a result of inhibition by soluble released products or exhaustion of available plastic substrate. It is interesting to note that during evolution, *Is*PETase libraries were analysed over time frames ranging from 3 to 7 h, meaning that limited selection pressure was applied to catalyst longevity at elevated temperatures. We anticipate that adapting selection pressures during future rounds of evolution will lead to improved variants capable of operating efficiently at elevated temperatures for more extended periods.

To further explore the use of HotPETase, we next attempted to deconstruct commercial-grade PET materials. HotPETase can depolymerize milled bottle-grade PET (bgPET, 41.9% crystallinity, full material characterization can be found in Extended Data Table 1 and Supplementary Figs. 7 and 8), albeit with a reduced conversion compared to that observed with cryPET powder (Fig. 3) (9.7 and 2.8% with cryPET and bgPET, respectively). To showcase the selectivity achievable with biocatalytic depolymerizations, HotPETase was used to deconstruct a common laminated packaging tray lid composed of PET and polyethylene (PE) (1.6% crystallinity, thickness of 325 µm PET and 40 µm PE, Extended Data Table 1). This PET/PE laminate is challenging to recycle mechanically, and indeed is considered a pollutant in commercial recycling streams. The HotPETase enzyme is adept at selectively deconstructing the PET portion of this material. In this instance, the extent of depolymerization after 24 h is substantially improved at 60 versus 40 °C (9.2 versus 2.9 mM of soluble monomer products released, corresponding to a degree of depolymerization of 48.1 and 15.3%, respectively, Fig. 3a and Extended Data Fig. 5). Scanning electron microscopy (SEM) reveals significant pitting of the PET surface, whereas the PE surface appears unchanged, compared to control reactions run in the absence of enzyme (Fig. 3b and Supplementary Fig. 9). The patterns of PET surface erosion differ in samples depolymerized at 40 versus

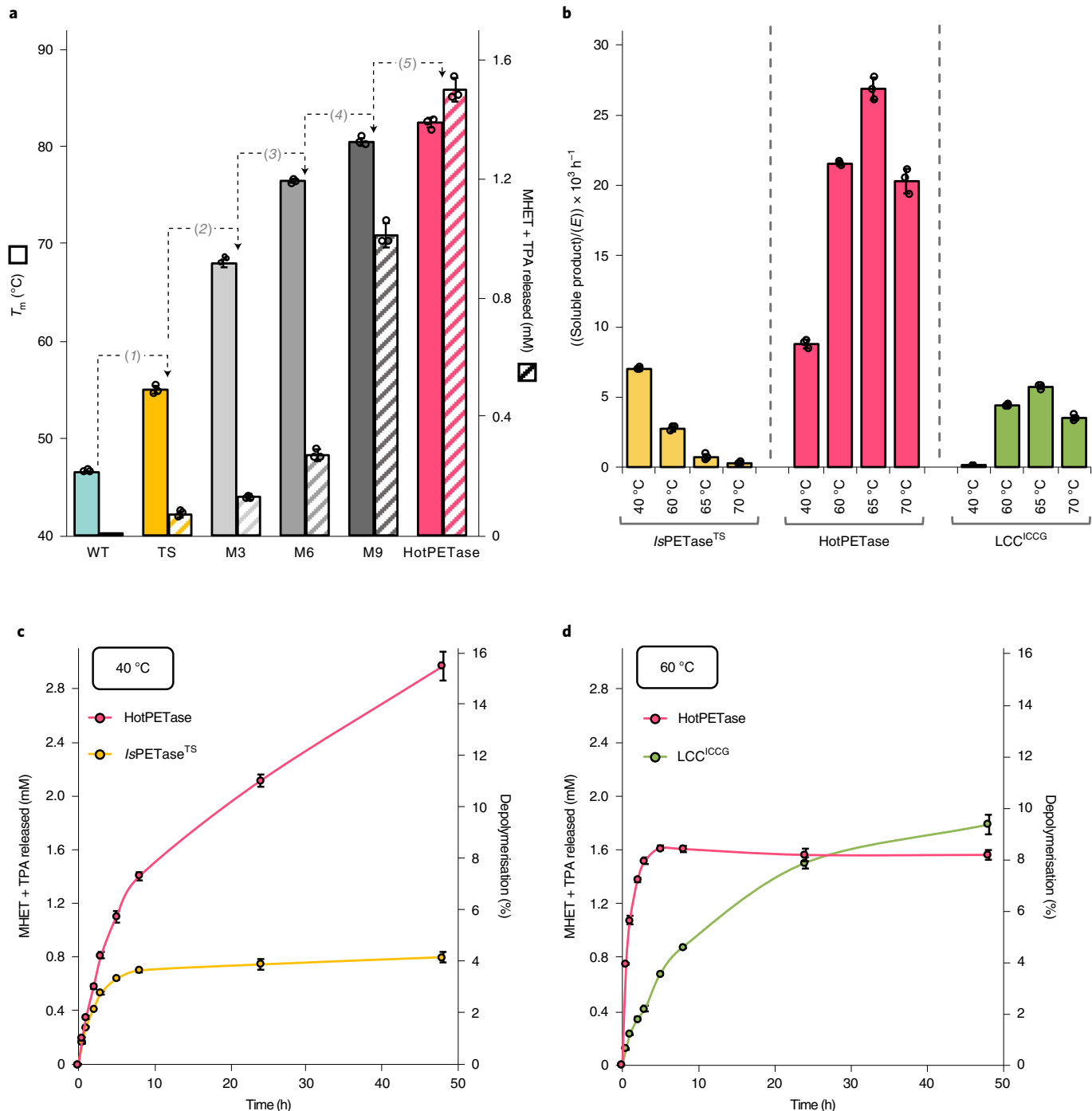


Fig. 2 | Directed evolution of *IsPETase*^{TS} afforded a more thermostable and active catalyst. **a**, Bar chart demonstrating a snapshot of protein variants along the evolutionary trajectory from *IsPETase*^{WT} to HotPETase. Protein variants are on the x axis; the mutations added to each variant in the bar chart compared to the previous variant are represented as follows: 1 is S121E, D186H, R280A; 2 is P181V, S207R, S214Y; 3 is Q119K, S213E, N233C, S282C; 4 is R90T, Q182M, N212K, R224L and 5 is S58A, S61V, K95N, M154G, N241C, K252M, T270Q. Solid coloured bars represent the mean T_m of each variant (left y axis). Hashed bars represent the mean concentration of MHET and TPA produced by each enzyme variant over the course of 48 h at 60 °C, using 0.4% cryPET by mass (4 g l^{-1}) and 0.29 mg enzyme per g PET (corresponding to 0.04 μM enzyme). **b**, Bar chart showing the mean enzyme turnovers per hour after 1 h of reaction, with cryPET substrate at different temperatures with *IsPETase*^{TS} (yellow), HotPETase (pink) or LCC^{ICCG} (green) as the biocatalyst, using 0.4% cryPET substrate loading (4 g l^{-1}) and 0.29 mg g^{-1} enzyme loading (0.04 μM). **c**, 48 h time-course reactions, with either HotPETase (pink) or *IsPETase*^{TS} (yellow), showing the mean total concentration of released MHET and TPA (left y axis) and mean percentage substrate depolymerized (right y axis) in reactions at 40 °C, using 0.4% cryPET substrate loading (4 g l^{-1}) and 0.29 mg g^{-1} enzyme loading (0.04 μM). **d**, 48 h time-course reactions with HotPETase (pink) or LCC^{ICCG} (green), showing the mean total concentration of released MHET and TPA (left y axis) and the mean percentage substrate depolymerized (right y axis) in reactions at 65 °C, using 0.4% cryPET substrate loading (4 g l^{-1}) and 0.29 mg g^{-1} enzyme loading (0.04 μM). For all reactions presented in this figure, *IsPETase* and its derivatives were assayed in the library screening buffer: pH 9.2, 50 mM Gly-OH with 4% BugBuster; LCC^{ICCG} was assayed in its reported optimal operating buffer: pH 8, 100 mM K-Pi¹⁶. Error bars represent the s.d. of triplicate measurements, each replicate measurement is represented with a black circle.

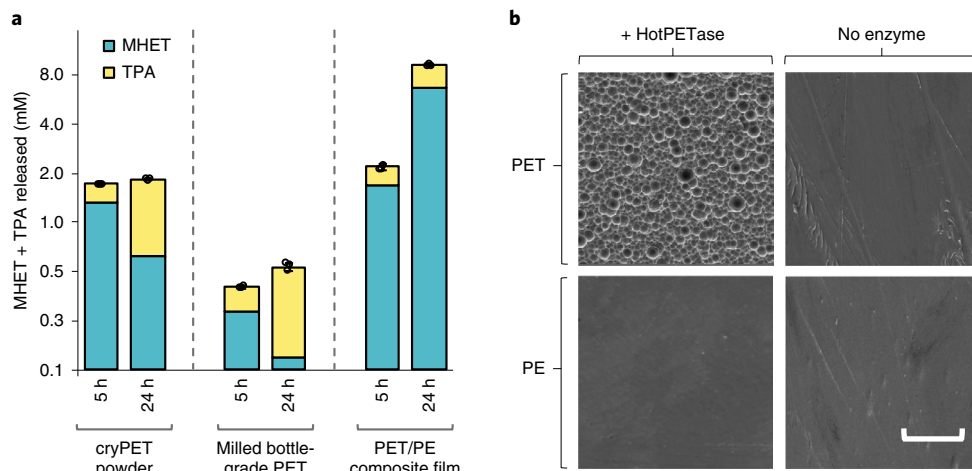


Fig. 3 | Biocatalytic deconstruction of a range of PET-based materials by HotPETase. **a**, Bar chart showing the mean concentration of released PET degradation products, MHET (blue) and TPA (yellow), produced following reaction of HotPETase at 60 °C over the course of 24 h, using 0.4% total substrate loading (4 g l⁻¹) and 0.29 mg g⁻¹ enzyme loading (0.04 μM). HotPETase has activity on crystalline PET powder (cryPET), milled bottle-grade PET (bgPET) and a PET/PE composite packaging tray lid (thickness of 325 μm PET and 40 μm PE, estimated 3.6 g l⁻¹ PET substrate loading). Assays were conducted under the library screening buffer conditions: pH 9.2, 50 mM Gly-OH buffer with 4% BugBuster. Reactions were carried out in triplicate; error bars represent the s.d. of the total MHET and TPA produced in the replicates; each replicate measurement is represented as a black circle. The y axis is on a logarithmic scale. Physical characterization of the substrates without treatment, incubated with buffer-only and postenzymatic deconstruction, is detailed in Extended Data Table 1. **b**, SEM images of both sides of a PET/PE packaging material degraded in the presence or absence of HotPETase, in a reaction at 40 °C over the course of 6 days. For the enzyme reaction, the PET/PE section (1.4% PET/PE film by mass (14 g l⁻¹), thickness of 325 μm PET and 40 μm PE, estimated 12.6 g l⁻¹ PET substrate loading) was submerged in a fresh solution of 0.08 mg g⁻¹ HotPETase (0.04 μM) and pH 9.2, 50 mM Gly-OH buffer with 4% BugBuster each day, leading to a 36.4% depolymerization of the PET portion of the sample. The no enzyme control was treated in the same manner, but with no enzyme applied. SEM images for reactions at 60 °C are provided in Supplementary Fig. 9. Five images were collected for each experiment, with those shown being representative of the set. Scale bar, 50 μm.

60 °C, with defined pits observed at 40 °C compared with a more rugged surface at the higher temperature (Supplementary Fig. 9). These differences could plausibly arise due to different rates and extents of polymer deconstruction at the two temperatures, or due to increased chain mobility at 60 versus 40 °C.

To improve the rate and extent of PET depolymerization achievable with HotPETase, we next optimized several reaction parameters including pH, reaction buffer, substrate loading and enzyme loading (Supplementary Figs. 10–12). Under optimal conditions using 3.62 mg g⁻¹ HotPETase enzyme loading (0.5 μM) and cryPET as the substrate (0.4% cryPET substrate loading (4 g l⁻¹), 20 mg total), 6.07 mM of soluble monomer products were formed (MHET:TPA ratio of 1:0.29) within 5 h at 60 °C, corresponding to a degree of depolymerization of 31% (Extended Data Fig. 6). Differential scanning calorimetry (DSC) analysis of samples before and after depolymerization show an overall increase in crystallinity from 29.8 to 41.7%, suggesting that HotPETase preferentially degrades the amorphous PET domains (Supplementary Fig. 13a and Extended Data Table 2). Size-exclusion chromatography (SEC) analysis shows no substantive change in the molecular weight and dispersity of the remaining PET (Supplementary Fig. 13b), which may indicate that the enzyme operates in an exo-cleavage fashion, depolymerizing individual polymer chains fully before chain transfer to a new macromolecule, thus retaining the original chain lengths in the bulk of the sample. Applying the optimized reaction conditions for cryPET depolymerization to alternative PET materials (bgPET and PET/PE laminate film) fails to enhance the rate or extent of depolymerization at 60 °C (Extended Data Fig. 5), suggesting that optimal process conditions are highly dependent on the characteristics of the material undergoing deconstruction.

Structural analysis. To gain insights into the origins of HotPETase thermostability and its improved activity, the crystal structure of the enzyme was solved and refined to a resolution of 2.2 Å for

comparison to the starting variant *IsPETase^{TS}*. The structures of HotPETase (Protein Data Bank (PDB) 7QVH) and *IsPETase^{TS}* (PDB 6IJ6) superimpose well, with a root-mean-square-deviation of 1.18 Å (Extended Data Fig. 7a). In HotPETase, the disulfide bridge between the Cys233 and Cys282 pair is formed as intended, with an S–S interatomic distance of 2.03 Å (Extended Data Fig. 7b). The P181V mutation results in an additional hydrogen bond between Val181 and Leu199 leading to better packing of the central β-sheet region compared to *IsPETase^{TS}* (Extended Data Fig. 7c and Supplementary Fig. 14). Analysis of the surface charge distributions of HotPETase and *IsPETase^{TS}* reveals substantial changes, including in the putative polymer binding cleft (Supplementary Fig. 15). Ensemble refinements of *IsPETase^{TS}* and HotPETase demonstrates that regions Ala183 to Asn190 and Cys203 to Leu216 have substantially decreased flexibility in the evolved enzyme (Supplementary Fig. 16).

To understand how HotPETase interacts with PET oligomers, we performed in silico docking using distance restraints to the Ser160 catalytic nucleophile and the backbone amides of the oxyanion hole (Tyr87 and Met161). The lowest energy docking pose is shown in Fig. 4a, with the PET oligomer (2-hydroxyethyl-(monohydroxyethyl) terephthalate, 4PET) occupying a shallow, extended binding cleft. The ‘wobbling’ tryptophan, Trp185, a feature that is thought to aid substrate binding and catalysis in the wild-type enzyme^{20,35}, is present as a single conformer in *apo*-HotPETase and is suitably positioned to accommodate the docked 4PET in a productive pose for catalysis (Fig. 4b). Extensive remodelling of the loop region connecting β7–α5, including introduction of a bulky Tyr214, leads to a new π-stacking interaction with Trp185 that restricts its conformational freedom (Fig. 4b and Extended Data Fig. 7d). A hydrogen bonding network involving Trp185, Tyr214 and the terminal hydroxyl group of 4PET also contributes to the stabilization of the docked oligomer within the binding cleft.

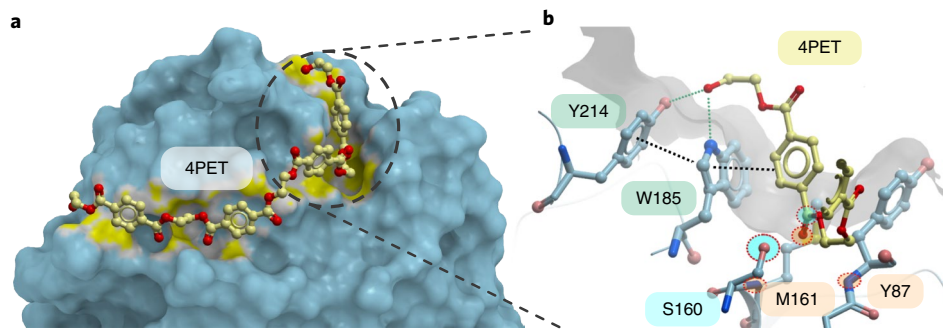


Fig. 4 | Structural characterization of HotPETase. **a**, Surface representation of HotPETase along with the top docking result of 4PET docked in ICM-Pro. The protein surface is coloured blue with contact patches between the docked 4PET and the surface highlighted in yellow. 4PET is shown in ball and stick representation coloured by all atom colours with pale yellow carbon atoms. **b**, A close up of the HotPETase catalytic site in conjunction with the docked 4PET structure. HotPETase residues are shown in ball and stick representation coloured by all atom colours with light blue carbon atoms. The docked 4PET is shown in ball and stick representation, coloured by all atom colours with pale yellow carbon atoms, with key hydrogen bonds highlighted as green dashed lines and π -stacking interactions shown as black dashed lines. The catalytic nucleophile (S160) and oxyanion hole (Y87, M161) are highlighted in cyan and orange, respectively (semitransparent spheres), along with their respective targets on the docked 4PET oligomer.

To explore the functional significance of the altered environment around Trp185 in HotPETase, residues installed in the β 7– α 5 connecting loop during evolution were reverted back to the amino acids present in the wild-type enzyme (HotPETase K212N, E213S, Y214S (HotPETase^{LR})). These modifications led to a substantial 7.5 °C reduction in T_m and compromised catalytic performance at elevated temperatures (Extended Data Fig. 8). Catalytic activity at low temperatures is minimally affected, suggesting that in the heavily engineered HotPETase, the fixed conformation of Trp185 is not detrimental to catalysis. Combined, these results indicate that a flexible Trp185 is not a prerequisite for efficient PET deconstruction.

Conclusions

The catalytic performances of PETases have previously been improved through rational engineering using computational methods, providing an important basis towards the development of commercially viable PET depolymerases. However, the engineering of industrial biocatalysts is most commonly achieved through directed evolution. The notable lack of PETases engineered using laboratory evolution probably reflects the challenges of developing suitable high-throughput, quantitative methods for analysing the catalytic deconstruction of insoluble polymers. Here, we have developed an automated directed evolution platform for engineering plastic deconstructing enzymes and showcase its use through the development of an evolved thermostable PETase (HotPETase, $T_m = 82.5$ °C), that can operate at the glass transition temperature of PET and depolymerizes semicrystalline PET more rapidly than previously reported PETases. HotPETase is able to deconstruct commercial bottle-grade PET and can selectively deconstruct PET in a PET/PE laminated packaging material, highlighting the potential benefits of enzymatic depolymerizations for real-world samples with minimal pretreatment or processing. Structural characterization of HotPETase highlights formation of the intended Cys233–Cys282 disulfide bridge and improved packing of the central β -sheet region, which probably aids thermostability, alongside the presence of a single well-defined conformer of Trp185, indicating that flexibility of this tryptophan is not a prerequisite for effective catalysis. To maximize the use of our platform moving forward, it will be important to interface our evolution methods with alternative strategies for augmenting biocatalyst function, including computationally guided engineering³⁶, introduction of polymer binding domains³⁷ and the development of multienzyme complexes³⁸. Likewise, combining and optimizing biocatalytic deconstructions with enzymatic monomer upcycling methods will be an important avenue for exploration^{39,40}.

In all cases, detailed techno-economic and life-cycle analysis will play a crucial role in assessing commercial viability, as well as defining target parameters for future biocatalyst engineering^{7,8}.

In the future, we anticipate that by adapting the selection pressures of our directed evolution workflows, we will be able to engineer a suite of useful biocatalysts with complementary functions and improved activities under process-relevant conditions. For example, we can extend catalyst stability and lifetime by increasing reaction times and temperatures, optimize biocatalysts to act on alternative plastic substrates or enhance enzyme specificities in order that they operate on single polymer components from mixed plastic waste streams. In doing so, our laboratory evolution platform will contribute to a biocatalytic recycling strategy to recover value from plastic waste.

Methods

Gene construction. The genes encoding *Is*PETase^{TS} (*Is*PETase S121E, D186H, R280A, signal sequence removed as by Son et al.⁴¹) and LCC^{ICCG} (LCC F243I, D238C, S283C, Y127G, signal sequence removed as by Tournier et al.⁴²) were commercially synthesized by Integrated DNA Technologies as gBlock fragments with codon optimization for expression in *Escherichia coli* cells. The *Is*PETase^{TS} gene was cloned into the NdeI (5' end) and XhoI (3' end) sites of a pBbE8K vector modified to contain a C-terminal hexa-histidine tag coding sequence following the XhoI restriction site⁴¹, to form pBbE8K_*Is*PETase^{TS}. The gene encoding LCC^{ICCG} was cloned into the NdeI (5' end) and XhoI (3' end) sites of pET-22b vector (Novagen) leading to fusion to a C-terminal hexa-histidine tag coding sequence, to form pET-22b_LCC^{ICCG}. Nucleotide sequences and expressed amino acid sequences of the genes used and plasmid maps of the vector constructs are provided in Supplementary Figs. 17–19.

Library construction. Rounds 1–6: iterative saturation mutagenesis. In each round, 24–30 residues were selected and individually randomized using cassette mutagenesis. Positions were chosen for mutation on the basis of a range of factors, detailed in Supplementary Table 1. For residue identification via the Protein One Stop Repair Shop webserver⁴², *Is*PETase^{WT} was used as the input protein (PDB 5XJH), with all constraints fixed to the default settings; positions identified more than twice by the software were selected for mutation. For residue identification via the B-fitter software⁴³, *Is*PETase^{WT} was again used as the input protein (PDB 5XJH); the 15 top positions ranked by highest B-factor were selected for mutation. DNA libraries at chosen residue positions were constructed via standard overlap-extension PCR, using degenerate primer pairs (containing an NNK codon at the position to be mutated) and pBbE8K_*Is*PETase^{TS} as the template for round 1, with the most active clone discovered at the end of each directed evolution cycle serving as the template for subsequent rounds. Primer sequences are provided in Supplementary Table 2.

Shuffling by overlap-extension PCR. After each round of evolution, beneficial diversity was combined by a process of DNA shuffling. Fragments were generated by overlap-extension PCR using designed primers that encoded for either an identified beneficial mutation or the parental amino acid. Using these primers,

up to six short fragments were created, DpnI digested, PCR-purified and mixed in appropriate combinations in overlap-extension PCRs. The resulting genes contained all possible combinations of mutations (from two to five mutations per gene) and were subsequently cloned into the pBbE8K vector as described previously.

Variant gene construction. HotPETase K212N, E213S, Y214S (HotPETase^{LR}), was created via overlap-extension PCR with HotPETase as the template protein and primers designed to encode the wild-type residues at positions 212–214. Primer sequences are provided in Supplementary Table 3. The resulting gene was cloned into the pBbE8K vector as described previously.

Protein production for library screening. For all protein expression and screening of libraries, transfer and aliquoting steps were performed using a Hamilton liquid-handling robot. pBbE8K_1sPETase libraries were expressed in chemically competent Origami 2 *E. coli* cells. Single colonies from a fresh transformation were used to inoculate 180 µl of Luria–Bertani (LB) media supplemented with 25 µg ml⁻¹ kanamycin (to maintain the pBbE8K_PETase plasmid) and 2.5 µg ml⁻¹ tetracycline (to maintain the glutathione reductase (*gor*) gene-containing plasmid present in Origami 2 cells), in 96-deep-well plates. Each plate contained six positive controls consisting of clones of the parent template, and two negative controls consisting of clones containing pBbE8K_RFP (red fluorescent protein). Plates were incubated overnight at 30 °C, 80% humidity in a shaking incubator (950 r.p.m.). Expression cultures were then prepared by inoculating 460 µl of 2YT media containing 25 µg ml⁻¹ kanamycin and 2.5 µg ml⁻¹ tetracycline with 40 µl of overnight culture in deep-well plates. The inoculated plates were incubated at 30 °C, 80% humidity in a shaking incubator (950 r.p.m.). When an optical density at 600 nm (OD₆₀₀) of 1 was reached, protein production was initiated by the addition of L-arabinose to a final concentration 10 mM and plates incubated for a further 20 h at 19 °C, 80% humidity in a shaking incubator (950 r.p.m.). Cells were collected by centrifugation at 2,900g for 10 min and the resulting pellets resuspended in a lysis mix consisting of 50 µl of BugBuster Protein Extraction reagent containing 10 µg ml⁻¹ DNase I. Cell lysis was initiated by incubation for 30 min at 30 °C, with 80% humidity in a shaking incubator (950 r.p.m.) and the lysate produced diluted with 300 µl of reaction buffer (pH 9.2, 50 mM glycine-OH (Gly-OH)). Insoluble cell debris was removed via centrifugation for 10 min at 2,900g to produce a clear cell lysate.

Production of purified proteins. 1sPETase and its derivatives were expressed in chemically competent Origami 2 *E. coli*. Single colonies of freshly transformed cells were cultured for 18 h at 30 °C in 5 ml of LB medium supplemented with 25 µg ml⁻¹ kanamycin and 2.5 µg ml⁻¹ tetracycline. 1 ml of the resulting culture was used to inoculate 50 ml of 2YT medium containing 25 µg ml⁻¹ kanamycin and 2.5 µg ml⁻¹ tetracycline. Cultures were grown at 35 °C, 180 r.p.m. to an OD₆₀₀ of 1. Protein production was initiated by the addition of L-arabinose (final concentration of 10 mM) and cultures then grown at 19 °C for 20 h. The *E. coli* cells were gathered by centrifugation at 3,220g for 10 min and resuspended in lysis buffer (pH 7.5, 50 mM Tris-HCl, 10 mM imidazole, 300 mM NaCl, 10 µg ml⁻¹ DNase I). Cells were disrupted by sonication and the resulting lysate clarified by centrifugation (13,500 for 15 min). The soluble fraction was subjected to affinity chromatography via application to Ni-NTA agarose (Qiagen). After washing off unbound proteins with the lysis buffer supplemented with 10 mM imidazole, bound proteins were eluted with elution buffer (pH 7.5, 50 mM Tris-HCl, 300 mM imidazole, 300 mM NaCl). Proteins were desalting by application to 10DG desalting columns (Bio-Rad) and eluted in storage buffer (pH 7.5, 50 mM Tris-HCl, 150 mM NaCl). Protein purity was confirmed by SDS-PAGE and concentrations determined by measuring the absorbance at 280 nm, assuming an extinction coefficient of 39,670 M⁻¹ cm⁻¹ for 1sPETase^{TS}-1sPETase^{M2}, 41,160 M⁻¹ cm⁻¹ for 1sPETase^{M3}-1sPETase^{M7} and 41,285 M⁻¹ cm⁻¹ for 1sPETase^{M8}-HotPETase.

For the cutinase, LCC^{ICCG}, the gene was expressed in chemically competent *E. coli* BL21 (DE3). Single colonies of freshly transformed cells were cultured for 18 h at 30 °C in 5 ml of LB medium supplemented with 25 µg ml⁻¹ ampicillin. 1 ml of the resulting culture was used to inoculate 50 ml of auto-inducible 2YT medium containing 25 µg ml⁻¹ ampicillin. Cultures were grown at 35 °C, 180 r.p.m., to an OD₆₀₀ of 1, and then cooled to 19 °C, for 20 h. Protein purification then proceeded as detailed for 1sPETase, with protein concentrations determined using an extinction coefficient of 37,150 M⁻¹ cm⁻¹. HotPETase exhibits a high-level of cytosolic protein expression (roughly 110 mg l⁻¹), LCC^{ICCG} has a lower level of protein expression (roughly 20 mg l⁻¹) (Supplementary Fig. 20).

Library screening using amorphous PET film (amoPET). The clarified cell lysate was incubated in foil-sealed plates for 30 min to 1 h at 55–80 °C (pre-incubation step) and subjected to centrifugation at 2,900g for 10 min to remove any insoluble protein precipitate formed. To initiate the PET degradation reaction, 60–220 µl of clarified cell lysate was transferred to a 96-deep-well plate containing reaction buffer (pH 9.2, 50 mM Gly-OH) and a single 6 mm amoPET disc cut from a sheet in each well, to make a final reaction volume of 220–400 µl. Lysate volume was varied across rounds to avoid overloading the UPLC column by keeping peak areas below 2,000 mAU and to limit evaporation at higher reaction temperatures and extended reaction times. Plates were then foil-sealed and incubated for 3–7 h

at 55–70 °C, after which reactions were terminated by the addition of an equal volume of a cold methanol and 12.5 mM trifluoroacetic acid solution. Following reaction quenching, plates were foil-sealed and incubated for 30 min at 30 °C, 80% humidity in a shaking incubator, 950 r.p.m. and insoluble protein precipitate removed by centrifugation for 10 min at 2,900g. A UPLC analysis sample was then prepared by transferring 100 µl of the resulting reaction supernatant into a fresh 96-well microtitre plate and the plate foil-sealed. The most active clones of each round were then subjected to a second screening round, where each clone was represented as a triplicate. All expression and screening protocols were as described above, apart from overnight culture preparation, where LB media was instead inoculated with 20 µl of a glycerol stock of the original overnight cultures from the library screening round. Details for the temperatures and lengths of the pre-incubation steps, the lysate volumes added to reactions, and the temperatures and lengths of the reaction incubations for each round of directed evolution are provided in Supplementary Table 1.

Purified protein screening using amorphous PET film (amoPET). AmoPET film assays with purified proteins were conducted as follows: a foil-sealed 96-deep-well plate containing the reaction buffer (library screening buffer, pH 9.2, 50 mM Gly-OH, 4% BugBuster, for 1sPETase and its derivatives, pH 8, 100 mM K-Pi, for LCC^{ICCG}, as reported in Tournier et al.^[16]), with a single 6 mm amoPET disc in each well, was incubated for 1 h at the reaction temperature (40–70 °C) to equilibrate all reaction components to the reaction temperature (equilibration step). For directed evolution hit retesting and beneficial diversity shuffling, purified proteins were incubated in foil-sealed plates for 30 min to 1 h at 55–80 °C before reaction set up (pre-incubation step, full details in Supplementary Table 1) and subjected to centrifugation at 2,900g for 10 min to remove any insoluble protein precipitate formed. The reaction was initiated by adding the purified enzymes to the prepared 96-deep-well plate containing reaction buffer and amoPET discs (final reaction conditions: 0.04 µM enzyme, 400 µl total volume). Protein variants were arrayed across the 96-deep-well plate in triplicate. Plates were foil-sealed and incubated for up to 24 h at the desired temperature, after which reactions were terminated by the addition of an equal volume of a cold methanol and 12.5 mM trifluoroacetic acid solution. Following reaction quenching, samples were incubated for 30 min at 30 °C, 80% humidity in a shaking incubator, 950 r.p.m. and insoluble protein precipitate removed by centrifugation for 10 min at 2,900g. A UPLC analysis sample was then prepared by transferring 100 µl of the resulting reaction supernatant into a fresh 96-well microtitre plate, and the plate foil-sealed.

Purified protein screening using crystalline PET powder (cryPET) and alternative PET substrates. Crystalline PET powder assays were conducted as follows: a 12 ml lidded glass vial containing 5 ml of reaction buffer (library screening buffer, pH 9.2, 50 mM Gly-OH, 4% BugBuster, for 1sPETase and its derivatives or pH 8, 100 mM K-Pi for LCC^{ICCG}), with 20 mg crystalline PET powder (cryPET) was incubated for 1 h at the reaction temperature (40–70 °C) to equilibrate all reaction components to the reaction temperature (equilibration step). The reaction was initiated by adding the purified protein (0.04 µM final concentration) coupled with incubation at the desired temperature under agitation at 180 r.p.m. Samples were taken at multiple time points, quenched and prepared for UPLC analysis as detailed previously. The percentage depolymerization of plastic was calculated using the mass of TPA and MHET produced, using the concentrations of each compound as determined by UPLC. For assays under optimized conditions, reactions were carried out as above, using a final enzyme concentration of 0.5 µM in pH 9.7, 50 mM Gly-OH buffer, 4% BugBuster.

For bottle-grade PET assays, bottle-grade PET pellets (bgPET, RamaPET N1) were micronized using a RETSCH PM100 Planetary Ball Mill at 500 r.p.m. for 30 min to form a powder. For PET/PE composite packaging tray lid assays, PET/PE composite packaging lids, thickness of 325 µm PET and 40 µm PE, were cut into 6-mm discs. For both materials, 20 mg of the resulting prepared substrates were used in reactions, with reaction conditions as described above. Full characterizations of the PET substrates described are detailed in Extended Data Table 1.

Chromatographic analysis of reactions. UPLC analysis was carried out on a 1290 Infinity II Agilent LC system including an autosampler with the ultraviolet detector set to 260 nm, using a Kinetex XB-C18 100 Å, 5 µm, 50 × 2.1 mm, LC Column with a stepped, isocratic solvent ratio method. Mobile phase A was water containing 0.1% formic acid and mobile phase B was acetonitrile with a fixed flow rate of 1.1 ml min⁻¹. Either 1 or 4 µl of sample was injected for library screening reactions or time-resolved purified protein assays, respectively. Following sample injection, the mobile phase was set to 13% buffer B for 52 s to separate TPA and MHET, stepped up to 95% buffer B for 33 s to separate larger reaction products and contaminants, and then stepped back down to 13% buffer B for column re-equilibration until a total run time of 1.8 min. Peaks were assigned by comparison to chemical standards prepared from commercial TPA and in-house synthesized MHET, and the peak areas integrated using Agilent OpenLab software. Using this method, TPA is eluted at roughly 0.4 min, MHET at around 0.6 min and small amounts of bis(2-hydroxyethyl) terephthalate (BHET) and longer oligomers at around 1–1.2 min (Supplementary Fig. 2). TPA and MHET concentrations were calculated by preparation of standard curves (Supplementary Fig. 21).

Characterization of PET substrates pre- and post-degradation. Polymer crystallinity was determined using DSC, using 4 mg of material. DSC data were obtained from using a DSC 2500 TA instrument. Samples were run in triplicate, in series, over a –50 to 300 °C temperature range under a nitrogen atmosphere at a heating rate of $\pm 10^\circ\text{C min}^{-1}$ in a 40 μl aluminium crucible. The number and weight average molecular weights (M_n and M_w) of polymer chains were determined by SEC. Samples (4 mg) were dissolved in hexafluoro-2-propanol (120 μl) at room temperature. Once dissolved, HPLC-grade chloroform (1,880 μl) was added to form a uniform, colourless solution that was filtered through a 0.24 μm polytetrafluoroethylene filter. SEC analysis was conducted on a system composed of an Agilent 1260 Infinity II LC system equipped with an Agilent guard column (PLGel 5 μm , 50 \times 7.5 mm) and two Agilent Mixed-C columns (PLGel 5 μm , 300 \times 7.5 mm). The mobile phase used was HPLC-grade CHCl₃ at 35 °C at flow rate of 1.0 ml min⁻¹. SEC samples were calibrated against linear polystyrene standards (162–2.4 \times 10⁵ g mol⁻¹).

SEM analysis of enzymatic depolymerizations of PET/PE composite packaging. A section of a PET/PE packaging lid (710 mg) was fully submerged in reaction buffer (pH 9.2, 50 mM Gly-OH, 4% BugBuster, 50 ml total) in a glass bottle, and HotPETase (0.04 μM final concentration) added to initiate the reaction. Reactions were incubated at either 40 or 60 °C with agitation at 120 r.p.m. The PET/PE packaging lid portion was washed and a fresh buffer and enzyme solution added each day over the course of 6 days. The control reactions were run in an identical manner, but with no enzyme added. The percentage depolymerization of the PET portion of each lid section was estimated from the release of MHET and TPA monomers, determined by UPLC analysis of the reaction supernatant taken each day, assuming an estimated 12.6 g l⁻¹ PET substrate loading. The extent of depolymerization was further confirmed by weight loss analysis of samples before and after biotransformations. Samples were analysed by SEM as follows: polymer samples were sputter coated with Au/Pd (thickness 5 nm) to prevent charging during SEM imaging and were observed using secondary electron imaging in a Tescan SC Mira, FEG-SEM with an accelerating voltage of 5 kV and probe current of approximately 2 nA.

Protein melting temperature (T_m) analysis. The melting temperatures (T_m) of *Is*PETase and its variants were determined using differential scanning fluorimetry. For each protein, a 50 μl sample of 5 μM protein was prepared in buffer (pH 9.2, 50 mM Gly-OH) with a final concentration of 10X SYPRO Orange dye stock solution (Sigma-Aldrich) in an optically clear, lidded PCR tube (Bio-rad). Differential scanning fluorimetry melt-curve experiments were conducted using a Bio-rad CFX Connect 96 Real-Time PCR system set on the fluorescence resonance energy transfer channel to use the 450/490 excitation and 560/580 emission filters. The temperature was increased from 25 to 95 °C with an increment of 0.3 °C s⁻¹. Each protein's T_m was determined from a mean value for the peak of the first derivative of the melt curve from three replicate measurements.

Structure determination of HotPETase. Protein crystallization of HotPETase was achieved by sitting drop vapour diffusion of 20 nl of 6 mg ml⁻¹ protein mixed with an equal volume of reservoir solution and incubated at 20 °C. Crystals were observed after 72 h incubation with a reservoir solution comprising 0.85 M sodium citrate tribasic dehydrate, 0.1 M Tris, pH 8.0 and 0.1 M sodium chloride (LMB screen HT96 H7 Molecular Dimensions). Before data collection, crystals were cryogenically protected with the addition of 20% PEG 200 to the mother liquor and plunge cooled in liquid nitrogen. All data were collected at Diamond Light Source. Data reduction was performed with Dials and the structure solved by molecular replacement using a search model derived from *Is*PETase^{WT} structure PDB 5XJH. Iterative rounds of model building and refinement were performed in COOT and Phenix using phenix.refine and phenix.ensemble_refinement. Validation with MOLPROBITY and PDBREDO were incorporated into the iterative rebuild and refinement process. Data collection and refinement statistics are shown in Supplementary Table 4. The HotPETase coordinates and structure factors have been deposited in the PDB under accession number 7QVH. The 4PET docking simulations were performed in ICM-Pro and resulted in a number of potential docked conformations. BHET was first docked into the active site using distance restraints to Ser160 and the backbone amides of the oxyanion hole to guide the docking towards catalytically plausible conformations. The position of the docked BHET was subsequently used as a template restraint for the larger 4PET docking. The top ranking docked pose of 4PET had an ICM VLS score of –31.

Reporting summary. Further information on research design is available in the Nature Research Reporting Summary linked to this article.

Data availability

Coordinates and structure factors have been deposited in the PDB under accession number 7QVH. Data supporting the findings of this study are available within the paper and its Supplementary Information, or are available from the authors upon reasonable request.

Received: 11 February 2022; Accepted: 22 June 2022;
Published online: 11 August 2022

References

- Geyer, R., Jambeck, J. & Law, K. Production, use, and fate of all plastics ever made. *Sci. Adv.* **3**, e1700782 (2017).
- Jambeck, J. R. et al. Plastic waste inputs from land into the ocean. *Science* **347**, 768–771 (2015).
- Laville, S. & Taylor, M. A million bottles a minute: world's plastic binge 'as dangerous as climate change'. *The Guardian* (28 June 2017).
- The New Plastics Economy: Rethinking the Future of Plastics & Catalysing Action* (Ellen MacArthur Foundation, 2017); <https://www.ellenmacarthurfoundation.org/publications/the-new-plastics-economy-rethinking-the-future-of-plastics-catalysing-action>
- Burgess, M., Holmes, H., Sharmina, M. & Shaver, M. P. The future of UK plastics recycling: one bin to rule them all. *Resour. Conserv. Recycl.* **164**, 105191 (2021).
- Rahimi, A. & García, J. M. Chemical recycling of waste plastics for new materials production. *Nat. Rev. Chem.* **1**, 0046 (2017).
- Ellis, L. D. et al. Chemical and biological catalysis for plastics recycling and upcycling. *Nat. Catal.* **4**, 539–556 (2021).
- Singh, A. et al. Techno-economic, life-cycle, and socioeconomic impact analysis of enzymatic recycling of poly(ethylene terephthalate). *Joule* **5**, 2479–2503 (2021).
- Jehanno, C. et al. Organocatalysed depolymerisation of PET in a fully sustainable cycle using thermally stable protic ionic salt. *Green. Chem.* **20**, 1205–1212 (2018).
- Karayannidis, G., Chatzivgoustis, A. P. & Achillas, D. Poly(ethylene terephthalate) recycling and recovery of pure terephthalic acid by alkaline hydrolysis. *Adv. Polym. Technol.* **21**, 250–259 (2002).
- Andrady, A. L. Assessment of environmental biodegradation of synthetic polymers. *J. Macromol. Sci. C* **34**, 25–76 (1994).
- Herrero Acero, E. et al. Enzymatic surface hydrolysis of PET: effect of structural diversity on kinetic properties of cutinases from *Thermobifida*. *Macromolecules* **44**, 4632–4640 (2011).
- Sulaiman, S. et al. Isolation of a novel cutinase homolog with polyethylene terephthalate-degrading activity from leaf-branch compost by using a metagenomic approach. *Appl. Environ. Microbiol.* **78**, 1556–1562 (2012).
- Kawai, F. et al. A novel Ca²⁺-activated, thermostabilized polyesterase capable of hydrolyzing polyethylene terephthalate from *Saccharomonospora viridis* AHK190. *Appl. Microbiol. Biotechnol.* **98**, 10053–10064 (2014).
- Ribitsch, D. et al. Hydrolysis of polyethylene terephthalate by *p*-nitrobenzyl esterase from *Bacillus subtilis*. *Biotechnol. Prog.* **27**, 951–960 (2011).
- Tournier, V. et al. An engineered PET depolymerase to break down and recycle plastic bottles. *Nature* **580**, 216–219 (2020).
- Zimmermann, W. Biocatalytic recycling of polyethylene terephthalate plastic. *Philos. Trans. R. Soc. A* **378**, 20190273 (2020).
- Yoshida, S. et al. A bacterium that degrades and assimilates poly(ethylene terephthalate). *Science* **351**, 1196–1199 (2016).
- Austin, H. P. et al. Characterization and engineering of a plastic-degrading aromatic polyesterase. *Proc. Natl Acad. Sci. USA* **115**, E4350–E4357 (2018).
- Han, X. et al. Structural insight into catalytic mechanism of PET hydrolase. *Nat. Commun.* **8**, 2106 (2017).
- Joo, S. et al. Structural insight into molecular mechanism of poly(ethylene terephthalate) degradation. *Nat. Commun.* **9**, 382 (2018).
- Ronkvist, Å. M., Xie, W., Lu, W. & Gross, R. A. Cutinase-catalyzed hydrolysis of poly(ethylene terephthalate). *Macromolecules* **42**, 5128–5138 (2009).
- Wei, R. & Zimmermann, W. Biocatalysis as a green route for recycling the recalcitrant plastic polyethylene terephthalate. *Microb. Biotechnol.* **10**, 1302–1307 (2017).
- Son, H. F. et al. Rational protein engineering of thermo-stable PETase from *Ideonella sakaiensis* for highly efficient PET degradation. *ACS Catal.* **9**, 3519–3526 (2019).
- Son, H. F. et al. Structural bioinformatics-based protein engineering of thermo-stable PETase from *Ideonella sakaiensis*. *Enzym. Microb. Technol.* **141**, 109656 (2020).
- Cui, Y. et al. Computational redesign of a PETase for plastic biodegradation under ambient condition by the GRAPE strategy. *ACS Catal.* **11**, 1340–1350 (2021).
- Ma, Y. et al. Enhanced poly(ethylene terephthalate) hydrolase activity by protein engineering. *Engineering* **4**, 888–893 (2018).
- Arnold, E. H. Directed evolution: bringing new chemistry to life. *Angew. Chem. Int. Ed.* **57**, 4143–4148 (2018).
- Zeymer, C. & Hilvert, D. Directed evolution of protein catalysts. *Annu. Rev. Biochem.* **87**, 131–157 (2018).
- Zhu, B., Wang, D. & Wei, N. Enzyme discovery and engineering for sustainable plastic recycling. *Trends Biotechnol.* **40**, 22–37 (2021).

31. Zhong-Johnson, E., Voigt, C. & Sinskey, A. An absorbance method for analysis of enzymatic degradation kinetics of poly(ethylene terephthalate) films. *Sci. Rep.* **11**, 928 (2021).
32. Then, J. et al. A disulfide bridge in the calcium binding site of a polyester hydrolase increases its thermal stability and activity against polyethylene terephthalate. *FEBS Open Bio.* **6**, 425–432 (2016).
33. Ügdüler, S. et al. Towards closed-loop recycling of multilayer and coloured PET plastic waste by alkaline hydrolysis. *Green. Chem.* **22**, 5376–5394 (2020).
34. Erickson, E. et al. Comparative performance of PETase as a function of reaction conditions, substrate properties, and product accumulation. *Chem. Sus. Chem.* **15**, e202101932 (2022).
35. Chen, C.-C. et al. General features to enhance enzymatic activity of poly(ethylene terephthalate) hydrolysis. *Nat. Catal.* **4**, 425–430 (2021).
36. Huang, P.-S., Boyken, S. E. & Baker, D. The coming of age of de novo protein design. *Nature* **537**, 320–327 (2016).
37. Dai, L. et al. Enhancing PET hydrolytic enzyme activity by fusion of the cellulose-binding domain of cellobiohydrolase I from *Trichoderma reesei*. *J. Biotechnol.* **334**, 47–50 (2021).
38. Knott, B. C. et al. Characterization and engineering of a two-enzyme system for plastics depolymerization. *Proc. Natl Acad. Sci. USA* **117**, 25476–25485 (2020).
39. Sadler, J. C. & Wallace, S. Microbial synthesis of vanillin from waste poly(ethylene terephthalate). *Green. Chem.* **23**, 4665–4672 (2021).
40. Rorrer, N. A. et al. Combining reclaimed PET with bio-based monomers enables plastics upcycling. *Joule* **3**, 1006–1027 (2019).
41. Anderson, J. C. et al. BglBricks: a flexible standard for biological part assembly. *J. Biol. Eng.* **4**, 1 (2010).
42. Goldenzweig, A. et al. Automated structure-and sequence-based design of proteins for high bacterial expression and stability molecular cell technology automated structure-and sequence-based design of proteins for high bacterial expression and stability. *Mol. Cell* **63**, 337–346 (2016).
43. Reetz, M. T. & Carballeira, J. D. Iterative saturation mutagenesis (ISM) for rapid directed evolution of functional enzymes. *Nat. Protoc.* **2**, 891–903 (2007).

Acknowledgements

We acknowledge generous support from the Biotechnology and Biological Sciences Research Council (David Phillips Fellowship grant no. BB/M027023/1 to A.P.G.), the European Research Council (ERC Starter grant no. 757991 to A.P.G.), the Medical Research Council and Buddi (MRC iCASE PhD funding to E.L.B.), the UK Catalysis Hub (funded through grant nos. EP/R026815/1, EP/K014706/2, EP/K014668/1, EP/K014854/1, EP/K014714/1 and EP/M013219/1), the EPSRC (grant no. EP/R031711/1 to

S.J.H. and S.R.), the Henry Royce Institute for Advanced Materials (funded through grant nos. EP/R00661X/1, EP/S019367/1, EP/P025021/1 and EP/P025498/1), and the ISCF Smart Sustainable Plastic Packaging fund (grant no. NE/V01045X/1 with H. Holmes, M. Sharmina, A. Adelekan, T. Holmes). We are grateful to Diamond Light Source for time on beamlines i03, i04 and i04-1 under proposals MX12788-50, MX17773-25, MX17773-34 and MX17773-52, and to Manchester SYNBIOCHEM Centre (grant no. BB/M017702/1) and the Future Biomanufacturing Hub (EP/S01778X/1) for access to their facilities. The Graphical Abstract, Fig. 1 and Supplementary Fig. 9 were created with BioRender.com.

Author contributions

A.P.G. and E.L.B. designed and directed the research. E.L.B. carried out molecular biology, enzyme characterization, assay development, directed evolution experiments and interpreted and presented the data. E.L.B., R.S. and J.F. carried out protein production and purification and performed biochemical assays. R.S. carried out protein crystallization. P.J.R.D. discussed interpretations of biochemical assays. S.K. and M.P.S. carried out polymer characterization measurements and analysed and presented the associated data. S.R. and S.J.H. performed microscopy and interpreted the data. A.A.T. and A.A.G. carried out substrate milling. F.J.H. and C.L. interpreted, analysed and presented structural data, and carried out molecular docking studies. A.P.G., E.L.B., M.P.S. and S.K. wrote the manuscript. All authors discussed the results and reviewed the manuscript.

Competing interests

The authors declare no competing interests.

Additional information

Extended data are available for this paper at <https://doi.org/10.1038/s41929-022-00821-3>.

Supplementary information The online version contains supplementary material available at <https://doi.org/10.1038/s41929-022-00821-3>.

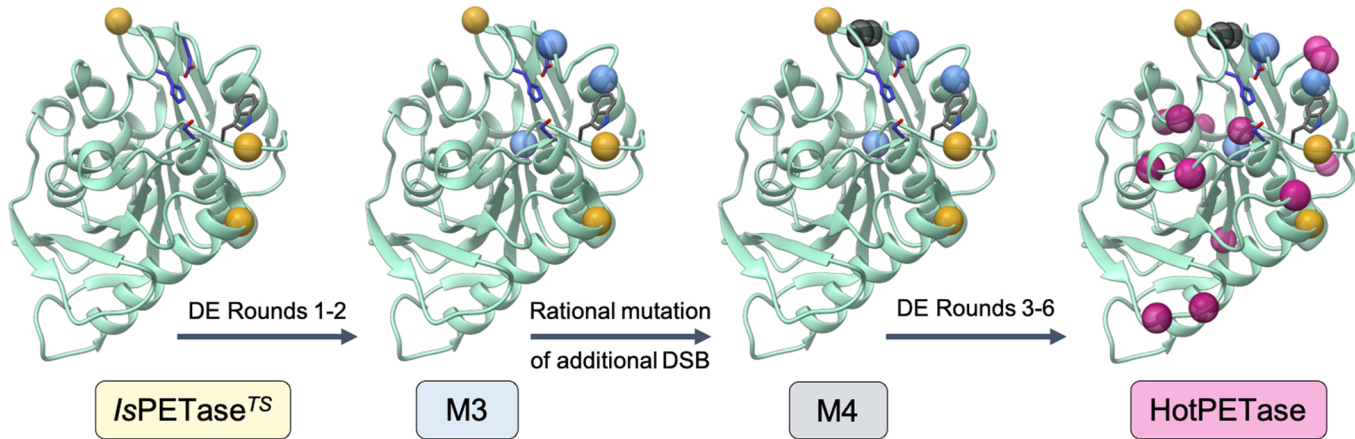
Correspondence and requests for materials should be addressed to Anthony P. Green.

Peer review information *Nature Catalysis* thanks Rey-Ting Guo, Ioannis Pavlidis and the other, anonymous, reviewer(s) for their contribution to the peer review of this work.

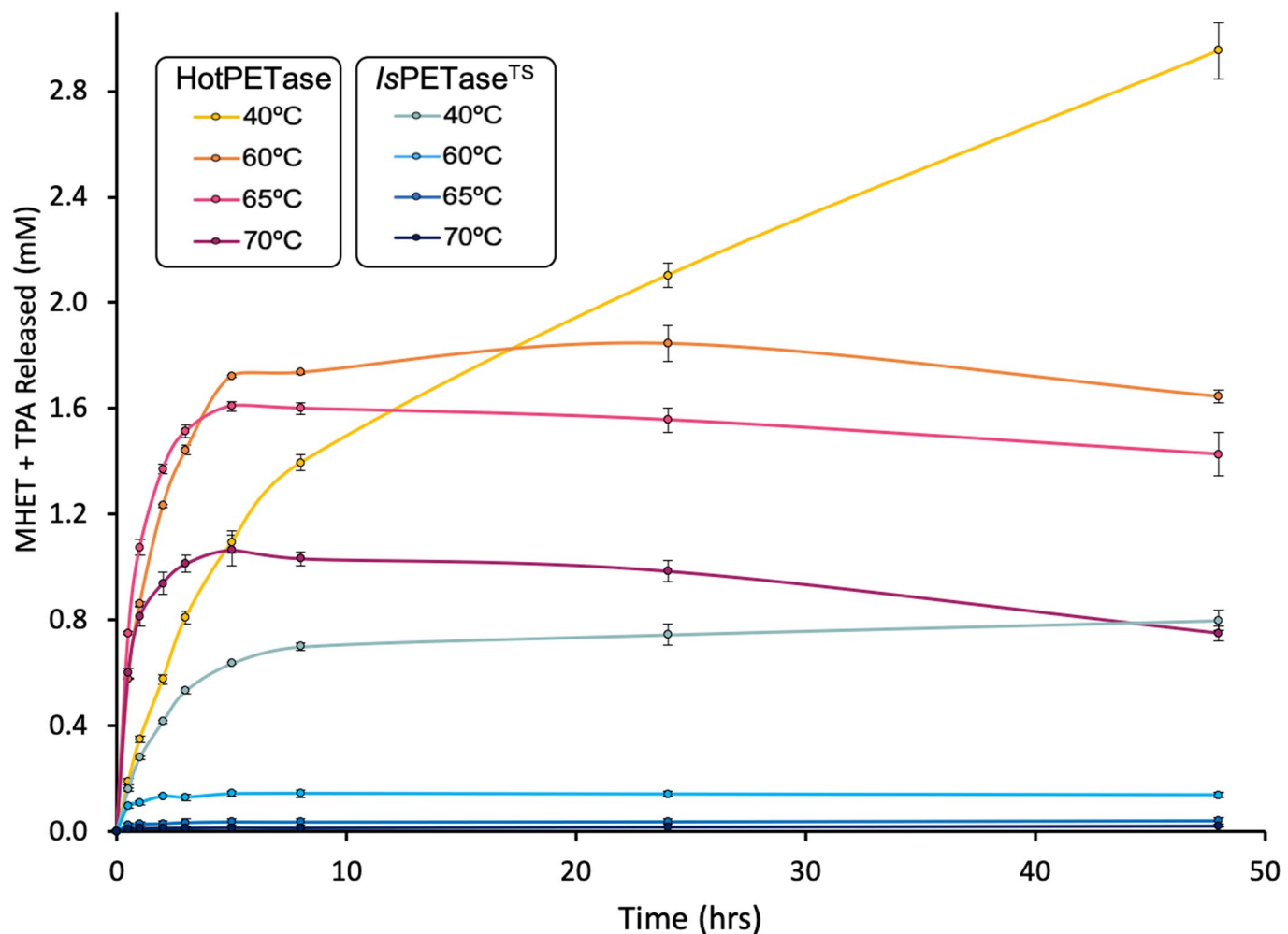
Reprints and permissions information is available at www.nature.com/reprints.

Publisher's note Springer Nature remains neutral with regard to jurisdictional claims in published maps and institutional affiliations.

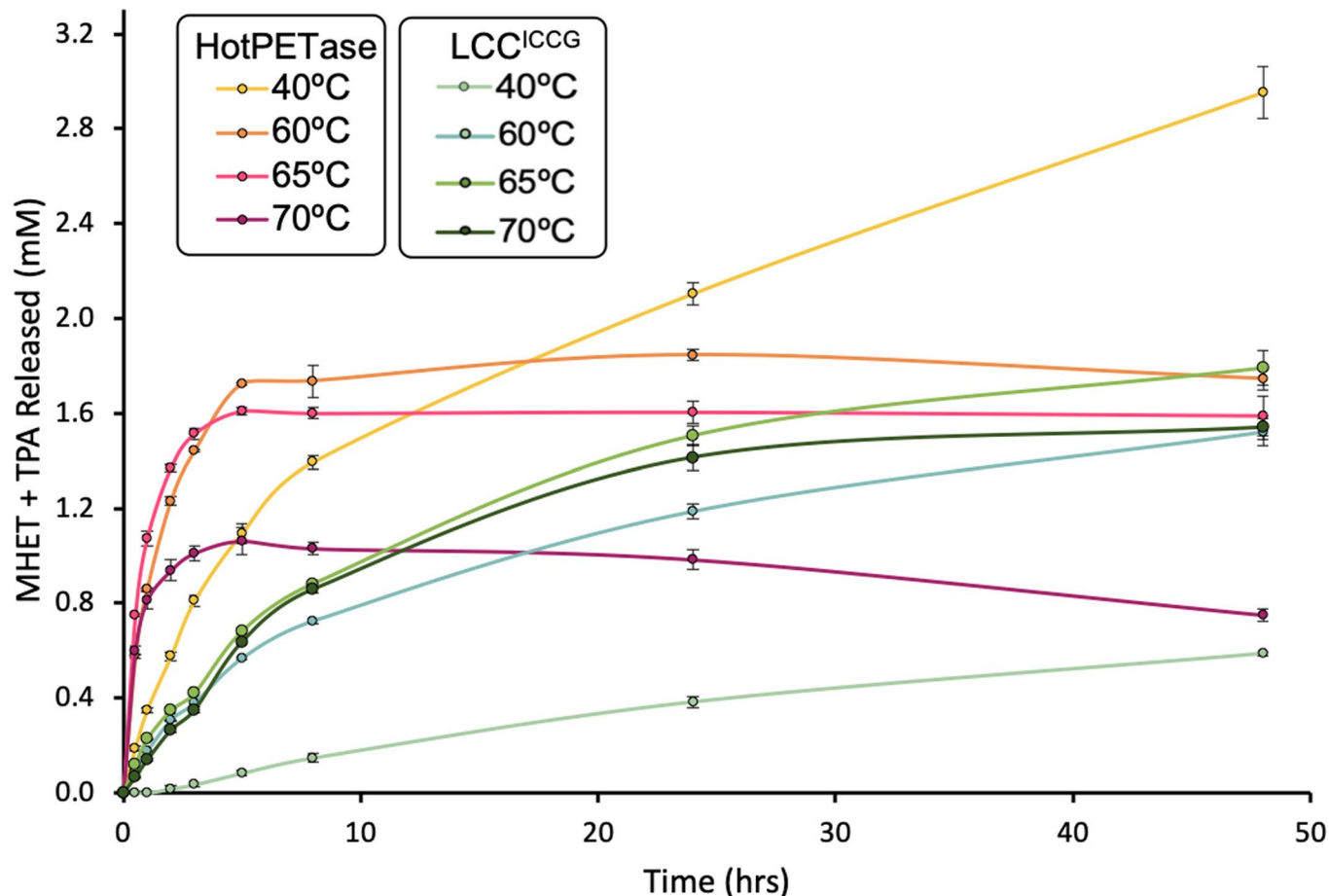
© Crown 2022



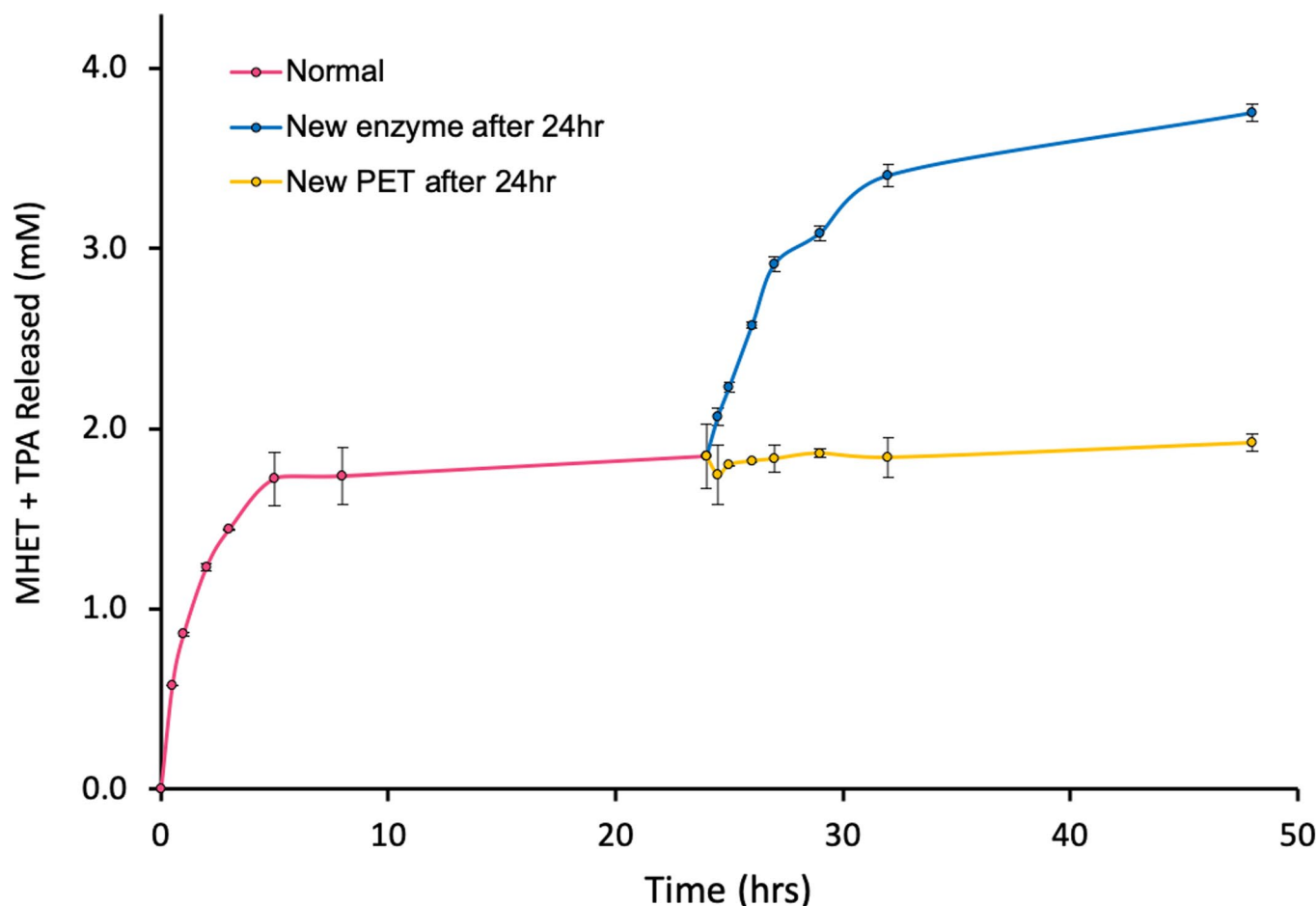
Extended Data Fig. 1 | Overview of the *IsPETase* directed evolution progression. The crystal structures represent an overview of the evolution, with the *IsPETase*^{TS} protein represented as a turquoise ribbon. The catalytic triad and W185 are shown in ball and stick representation coloured by all atoms, with blue and grey carbon atoms, respectively. The three mutations in *IsPETase*^{TS} compared to *IsPETase*^{WT} are highlighted as yellow spheres, mutations installed in directed evolution rounds 1-2 as light blue spheres, the rationally inserted additional disulphide bridge (DSB) as black spheres and mutations installed in rounds 3-6 as pink spheres. More details on the evolution outcomes can be found in Supplementary Table 1.



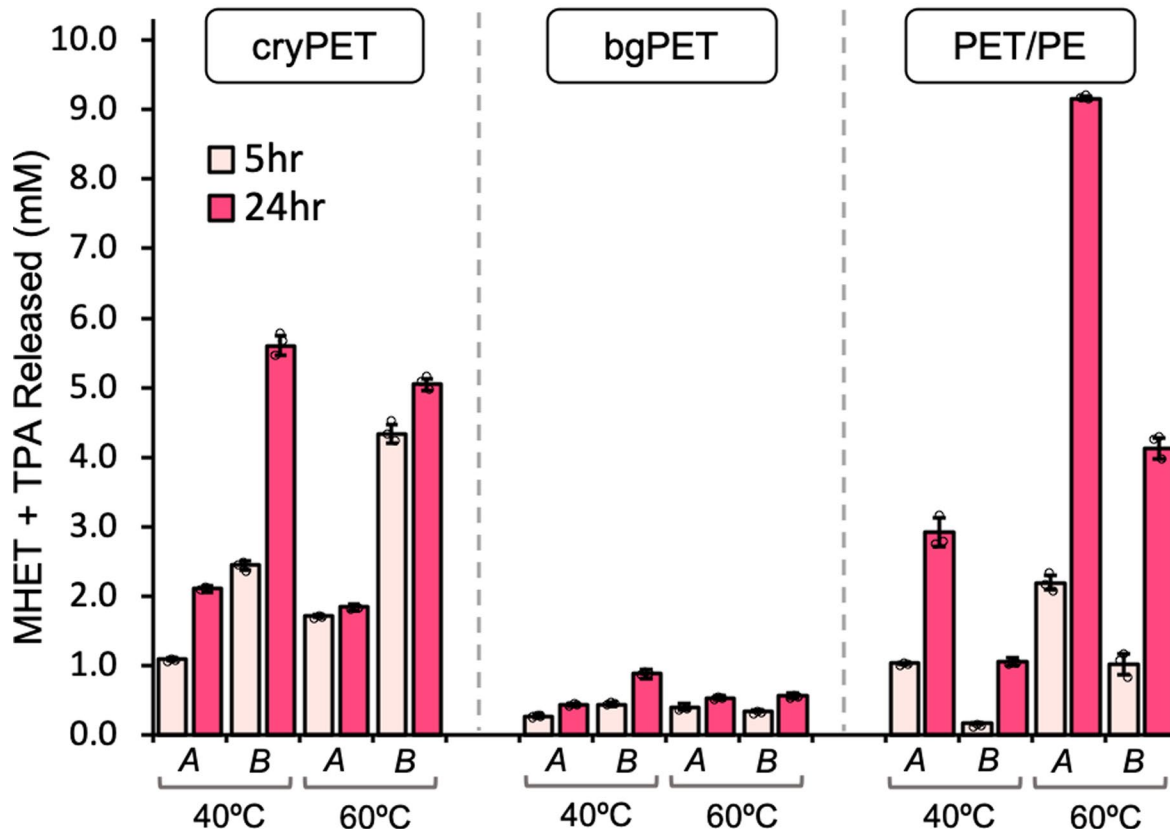
Extended Data Fig. 2 | Comparison of reactions with *lsPETase^{TS}* and HotPETase over a range of temperatures. 48 h time-courses of cryPET reactions, showing the mean total concentration of released MHET and TPA, with HotPETase (yellow-pink) and *lsPETase^{TS}* (blues) over time, using 0.4% cryPET substrate loading (4 g L^{-1}) and 0.29 mg g^{-1} enzyme loading ($0.04 \mu\text{M}$). Reactions were performed in pH 9.2, 50 mM Gly-OH buffer, 4% BugBuster, in triplicate, with error bars representing the s.d. of the replicate measurements.



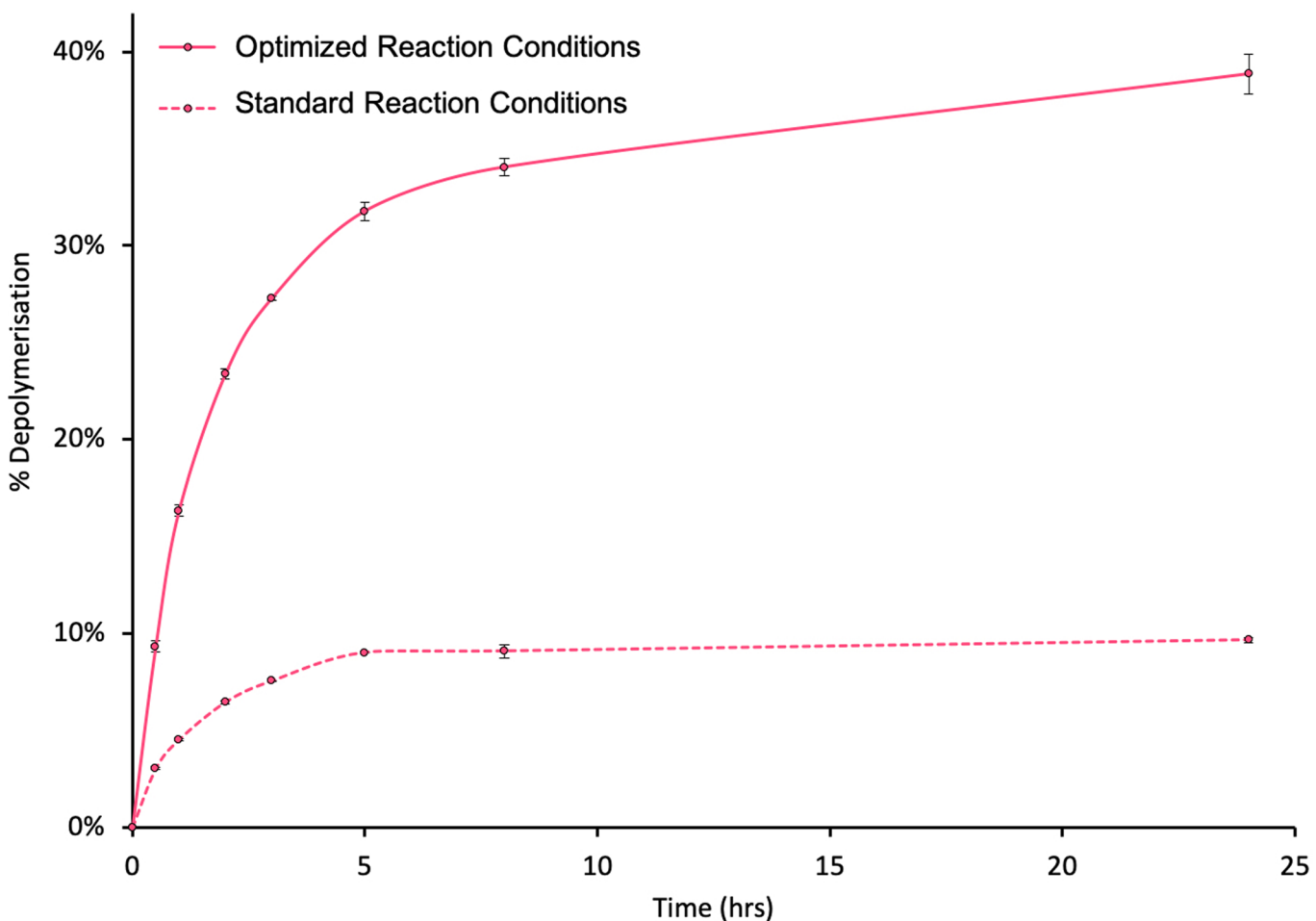
Extended Data Fig. 3 | Comparison of reactions with HotPETase and LCC^{ICCG} over a range of temperatures. 48 h time-courses of cryPET reactions, showing the mean total concentration of released MHET and TPA, with HotPETase (yellows-pinks) and LCC^{ICCG} (greens) over time, at a range of temperatures, using 0.4% cryPET substrate loading (4 g L^{-1}) and 0.29 mg g^{-1} enzyme loading ($0.04 \mu\text{M}$). LCC^{ICCG} was assayed in its reported optimal operating buffer: pH 8, 100 mM K-Pi; *Is*PETase and its derivatives were assayed under the library screening buffer conditions: pH 9.2, 50 mM Gly-OH buffer, 4% BugBuster. Reactions were carried out in triplicate, with error bars representing the s.d. of the replicate measurements.



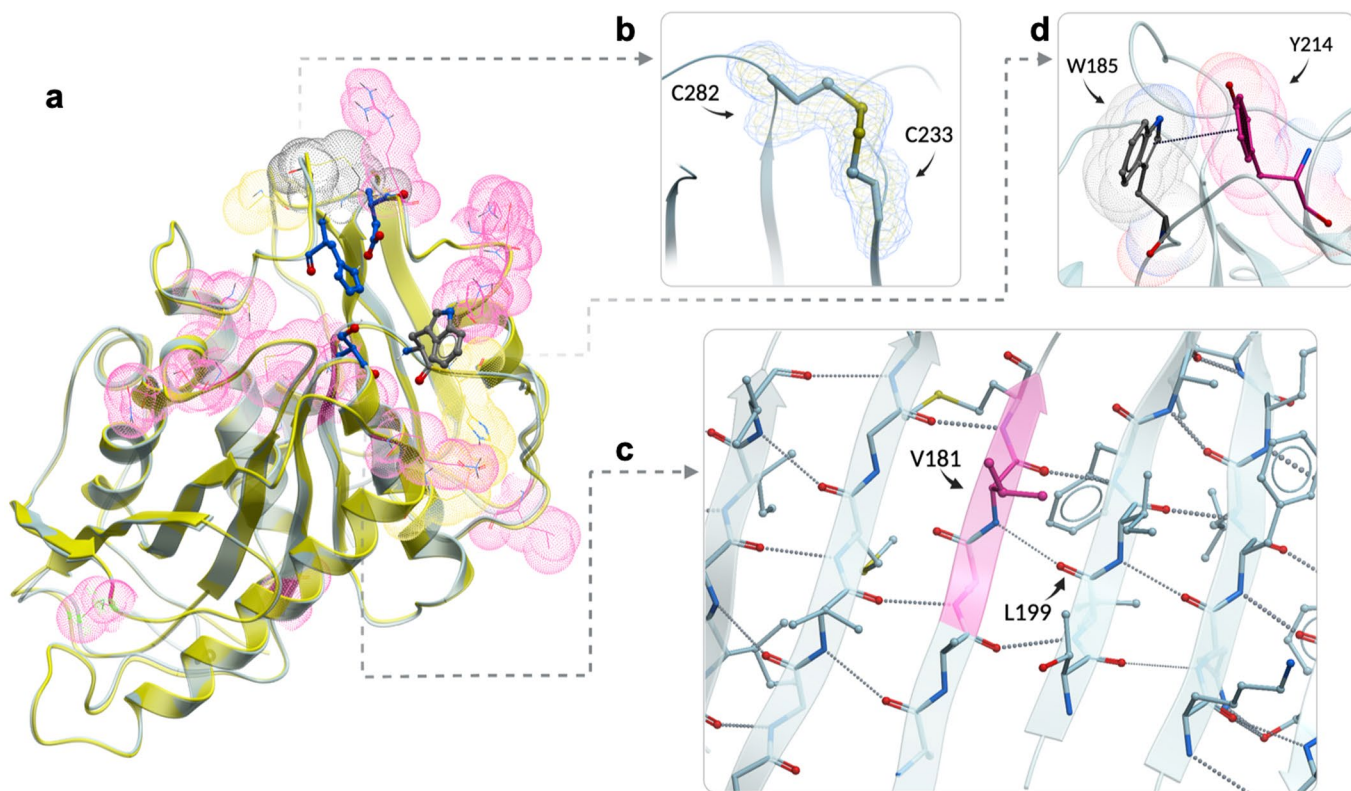
Extended Data Fig. 4 | Comparison of reactions with additional enzyme or substrate added. 48 h time-courses showing the mean total concentration of released MHET and TPA, where following reaction with HotPETase at 60 °C for 24 h (pink) (using 0.4% cryPET substrate loading (4 g L⁻¹) and 0.29 mg g⁻¹ enzyme loading (0.04 μM)), either 0.29 mg g⁻¹ fresh enzyme (0.04 μM) (blue) or 4 g L⁻¹ fresh cryPET substrate (yellow) was added. Reactions were performed in pH 9.2, 50 mM Gly-OH buffer, 4% BugBuster, in triplicate, with error bars representing the s.d. of the replicate measurements.



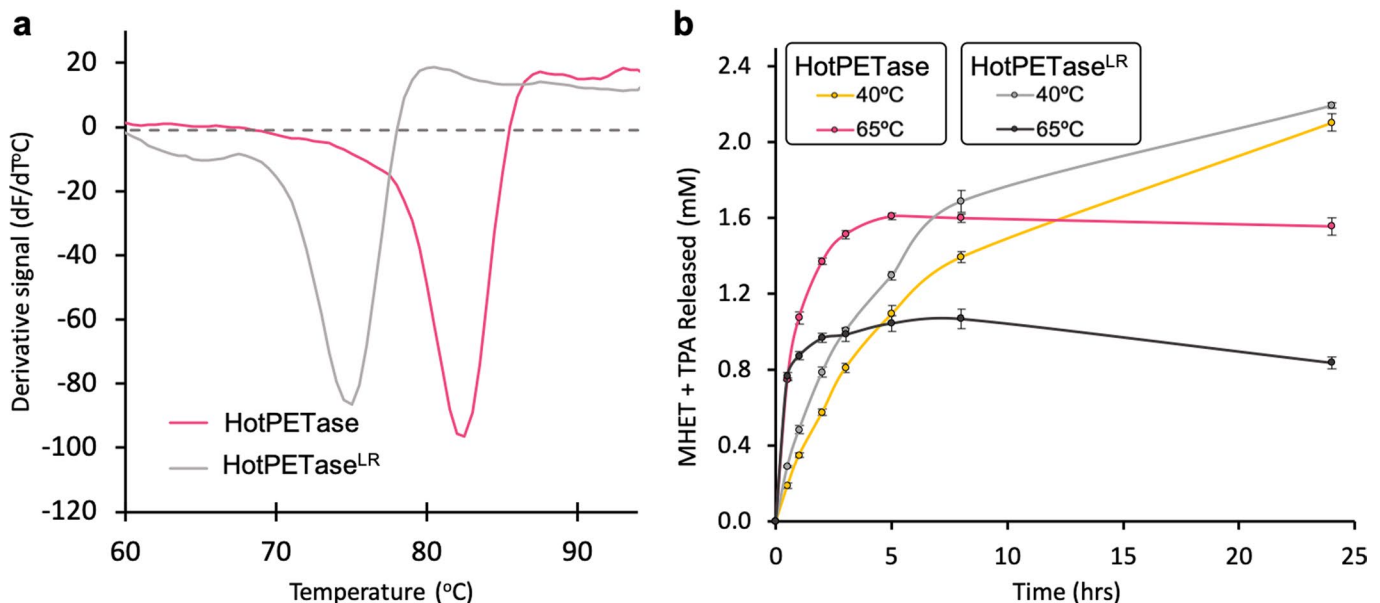
Extended Data Fig. 5 | Comparison of HotPETase activity with different substrates at 40 °C and 60 °C under library screening conditions and optimised reaction conditions. Bar chart showing the mean total concentration of released MHET and TPA accumulated over 3 h (light pink) and 24 h (dark pink) at either 40 °C or 60 °C in reactions using HotPETase with different PET substrates (crystalline PET powder (cryPET), milled bottle-grade PET (bgPET), PET/PE composite film lid (PET/PE), 0.4% total substrate loading (4 g L⁻¹)). Reactions were performed using either library hit screening conditions (A): 0.29 mg g⁻¹ enzyme loading (0.04 µM), pH 9.2, 50 mM Gly-OH, 4% BugBuster or optimised conditions (B): 3.62 mg g⁻¹ enzyme loading (0.5 µM), pH 9.7, 50 mM Gly-OH buffer, 4% BugBuster. Reactions were carried out in triplicate; error bars represent the s.d. of the replicate measurements; each replicate measurement is represented as a black circle.



Extended Data Fig. 6 | Comparison HotPETase activity under standard and optimised reaction conditions. 24 h time-courses of reactions conducted at 60 °C with HotPETase, showing the mean percentage of cryPET depolymerized (0.4% cryPET substrate loading (4 g L^{-1})), calculated using the concentration of MHET and TPA produced. Standard conditions were: 0.29 mg g^{-1} enzyme loading ($0.04\text{ }\mu\text{M}$), library screening buffer: pH 9.2, 50 mM Gly-OH, 4% BugBuster (dashed line). Optimised reaction conditions were: 3.62 mg g^{-1} enzyme loading ($0.5\text{ }\mu\text{M}$), pH 9.7, 50 mM Gly-OH, 4% BugBuster (solid line). Reactions were carried out in triplicate; error bars represent the s.d. of the replicate measurements.



Extended Data Fig. 7 | Comparison of crystal structures and features of HotPETase and *ls*PETase^{TS}. **(a)** A global superposition of *ls*PETase^{TS} (yellow) and HotPETase (light blue). Mutations in *ls*PETase^{TS} compared to *ls*PETase^{WT} are highlighted with yellow spheres. Mutations installed during directed evolution are highlighted with pink spheres. The rationally inserted disulphide bridge is highlighted with black spheres. The catalytic triad and W185 are in ball and stick representation coloured by all atoms, with blue and grey carbon atoms, respectively. **(b)** The disulphide bridge is correctly formed between C233 and C282 in HotPETase. Electron density is 2Fo-Fc contoured at 1 sigma (blue) and 2 sigma (yellow). **(c)** The conversion of P181 in *ls*PETase^{TS} to V181 in HotPETase (highlighted pink) results in extension of β -sheet 6, and the formation of an additional hydrogen bond (dashed lines) to L199. **(d)** In HotPETase, the wobbling tryptophan (W185, grey sticks), forms a π -stacking interaction (dashed line) with the installed Y214 (pink sticks).



Extended Data Fig. 8 | Comparison of HotPETase and HotPETase^{LR}. **(a)** Protein melt curves for HotPETase and HotPETase K212N, E213S, Y214S (HotPETase^{LR}). Melt curve readings were carried out in triplicate. **(b)** 24 h time-courses, showing the mean total concentration of released MHET and TPA, in reactions at either 40 °C or 65 °C with either HotPETase or HotPETase^{LR}, using 0.4% cryPET substrate loading (4 g L⁻¹) and 0.29 mg g⁻¹ enzyme loading (0.04 μM). Reactions were performed in pH 9.2, 50 mM Gly-OH buffer, 4% BugBuster, in triplicate; error bars represent the s.d. of the replicate measurements.

Extended Data Table 1 | PET substrate characterization before and after enzyme reactions

Substrate	Treatment	% Crystallinity	M _w (kDa)	M _n (kDa)	Dispersity
Amorphous PET film (amoPET)	No Treatment	6.7	58.0	22.4	2.51
	Buffer-Only Control	6.6	57.1	21.1	2.71
	Enzyme Reaction	8.4	57.3	20.5	2.79
Crystalline PET powder (cryPET)	No Treatment	29.8	83.3	34.6	2.40
	Buffer-Only Control	32.7	77.9	29.7	2.62
	Enzyme Reaction	38.2	80.5	30.2	2.78
Milled bottle-grade PET (bgPET)	No Treatment	39.9	72.2	23.9	2.77
	Buffer-Only Control	40.4	74.1	27.8	2.65
	Enzyme Reaction	41.3	76.1	30.2	2.51
PET/PE composite film	No Treatment	1.5	56.3	21.0	2.73
	Buffer-Only Control	6.1	52.9	19.4	2.73
	Enzyme Reaction	13.6	52.1	19.7	2.65

PET substrates were characterised pre-reaction (no treatment), following incubation in reaction buffer (buffer-only control) or following enzymatic depolymerization (enzyme reaction). Enzymatic reactions were conducted for 48 h with HotPETase at 60 °C, using 0.4% cryPET substrate loading (4 g L⁻¹) and 0.29 mg g⁻¹ enzyme loading (0.04 µM). Reactions were performed in pH 9.2, 50 mM Gly-OH buffer, 4% BugBuster. The negative, buffer-only control was prepared in a similar fashion without the addition of HotPETase. Crystallinity was assessed by DSC and molecular weights by SEC.

Extended Data Table 2 | Characterisation of cryPET substrate depolymerization under optimised conditions

Substrate	Treatment	% Crystallinity	M_w (kDa)	M_n (kDa)	Dispersity
Crystalline PET powder (cryPET)	No Treatment	29.8	83.3	34.6	2.40
	Buffer-Only Control	32.7	77.9	29.7	2.62
	Enzyme Reaction	41.7	78.2	28.1	2.78

CryPET substrate was characterised pre-reaction (no treatment), following incubation in reaction buffer (buffer-only control) or following enzymatic depolymerization (enzyme reaction). Enzymatic reactions were conducted for 48 h with HotPETase at 60 °C, using 0.4% cryPET substrate loading (4 g L⁻¹), 3.62 mg g⁻¹ enzyme loading (0.5 μM), pH 9.7, 50 mM Gly-OH, 4% BugBuster. The negative, buffer-only control was prepared in a similar fashion without the addition of HotPETase. Crystallinity was assessed by DSC and molecular weights by SEC.

Corresponding author(s): Anthony Green

Last updated by author(s): Jun 10, 2022

Reporting Summary

Nature Portfolio wishes to improve the reproducibility of the work that we publish. This form provides structure for consistency and transparency in reporting. For further information on Nature Portfolio policies, see our [Editorial Policies](#) and the [Editorial Policy Checklist](#).

Statistics

For all statistical analyses, confirm that the following items are present in the figure legend, table legend, main text, or Methods section.

n/a Confirmed

- The exact sample size (n) for each experimental group/condition, given as a discrete number and unit of measurement
- A statement on whether measurements were taken from distinct samples or whether the same sample was measured repeatedly
- The statistical test(s) used AND whether they are one- or two-sided
Only common tests should be described solely by name; describe more complex techniques in the Methods section.
- A description of all covariates tested
- A description of any assumptions or corrections, such as tests of normality and adjustment for multiple comparisons
- A full description of the statistical parameters including central tendency (e.g. means) or other basic estimates (e.g. regression coefficient) AND variation (e.g. standard deviation) or associated estimates of uncertainty (e.g. confidence intervals)
- For null hypothesis testing, the test statistic (e.g. F , t , r) with confidence intervals, effect sizes, degrees of freedom and P value noted
Give P values as exact values whenever suitable.
- For Bayesian analysis, information on the choice of priors and Markov chain Monte Carlo settings
- For hierarchical and complex designs, identification of the appropriate level for tests and full reporting of outcomes
- Estimates of effect sizes (e.g. Cohen's d , Pearson's r), indicating how they were calculated

Our web collection on [statistics for biologists](#) contains articles on many of the points above.

Software and code

Policy information about [availability of computer code](#)

Data collection	<p>Residues of interest were identified using PROSS: the Protein Repair One-Stop Shop, a publically available web server tool: Goldenzweig, A. et al. Automated Structure- and Sequence-Based Design of Proteins for High Bacterial Expression and Stability. <i>Mol. Cell</i> 2016, 63 (2), 337–346, https://pross.weizmann.ac.il/step/pross-terms/, and B-Fitter a publically available protein analysis software: Reetz, M. T. & Carballeira, J. D. Iterative saturation mutagenesis (ISM) for rapid directed evolution of functional enzymes. <i>Nature Protocols</i> 2, 891–903 (2007). https://www.kofo.mpg.de/en/research/biocatalysis. These are cited within the text.</p> <p>X-ray crystallography data were collected at Diamond Light Source (Harwell, UK).</p> <p>NMR data was collected with a 400 MHz Bruker spectrometer.</p> <p>SEM imaging was carried out using a Tescan SC Mira, FEG-SEM with an accelerating voltage of 5 kV and probe current of ~2 nA.</p> <p>DSF melt-curve experiments were conducted using a Biorad CFX Connect 96 Real-Time PCR system with the manufacturer's software.</p> <p>DSC data was obtained from using a DSC 2500 TA instrument.</p> <p>SEC was performed on a system composed of an Agilent 1260 Infinity II LC system.</p> <p>UPLC analysis was performed on a 1290 Infinity II Agilent LC system.</p>
Data analysis	<p>Data reduction was performed with Dials and the structure solved by molecular replacement using a search model derived from IsPETaseWT structure 5XJH. Iterative rounds of model building and refinement were performed in COOT and Phenix using phenix.refine and phenix.ensemble_refinement. Validation with MOLPROBITY and PDBREDO were incorporated into the iterative rebuild and refinement process</p> <p>HPLC peak integrations were carried out using Agilent OpenLab software, HPLC peak area data were analyzed and visualised in Microsoft Excel.</p> <p>NMR Data were analyzed using Mestrenova software.</p> <p>DSF melt-curves were analyzed using Biorad CFX Manager software.</p> <p>DSC data were analyzed using TRIOS software (TA instruments).</p> <p>Crystallography visualisation was carried out in Chimera and ICM Broswer (Molsoft LLC).</p> <p>The graphical abstract, Figure 1 and Supplementary Figure 9 were created using Biorender.com.</p>

For manuscripts utilizing custom algorithms or software that are central to the research but not yet described in published literature, software must be made available to editors and reviewers. We strongly encourage code deposition in a community repository (e.g. GitHub). See the Nature Portfolio [guidelines for submitting code & software](#) for further information.

Data

Policy information about [availability of data](#)

All manuscripts must include a [data availability statement](#). This statement should provide the following information, where applicable:

- Accession codes, unique identifiers, or web links for publicly available datasets
- A description of any restrictions on data availability
- For clinical datasets or third party data, please ensure that the statement adheres to our [policy](#)

Coordinates and structure factors for HotPETase have been deposited in the Protein Data Bank under accession number PDB: 7QVH. PDB 6IJ6 and PDB 5XJH were also used in the study for comparisons.

Field-specific reporting

Please select the one below that is the best fit for your research. If you are not sure, read the appropriate sections before making your selection.

Life sciences Behavioural & social sciences Ecological, evolutionary & environmental sciences

For a reference copy of the document with all sections, see nature.com/documents/nr-reporting-summary-flat.pdf

Life sciences study design

All studies must disclose on these points even when the disclosure is negative.

Sample size	For enzymatic assays and Tm measurements the standard sample size was n=3, to allow the calculation of a mean and standard deviation. For some experiments in the Supplementary information n=2 was used to allow the calculation of an average. Results were reproducible, standard deviations were small and the replication of experiments was successful.
Data exclusions	None excluded
Replication	All results in triplicate or duplicate and stated, from which a mean and standard deviation were calculated. Standard deviations were small and replication of experiments was successful.
Randomization	Data was not subjected to randomization as it was not applicable to the experiments carried out.
Blinding	For substrate characterization, SEM imaging and HPLC analysis, the researchers were blinded as to which samples were being analyzed.

Reporting for specific materials, systems and methods

We require information from authors about some types of materials, experimental systems and methods used in many studies. Here, indicate whether each material, system or method listed is relevant to your study. If you are not sure if a list item applies to your research, read the appropriate section before selecting a response.

Materials & experimental systems

n/a	Involved in the study
<input checked="" type="checkbox"/>	<input type="checkbox"/> Antibodies
<input checked="" type="checkbox"/>	<input type="checkbox"/> Eukaryotic cell lines
<input checked="" type="checkbox"/>	<input type="checkbox"/> Palaeontology and archaeology
<input checked="" type="checkbox"/>	<input type="checkbox"/> Animals and other organisms
<input checked="" type="checkbox"/>	<input type="checkbox"/> Human research participants
<input checked="" type="checkbox"/>	<input type="checkbox"/> Clinical data
<input checked="" type="checkbox"/>	<input type="checkbox"/> Dual use research of concern

Methods

n/a	Involved in the study
<input checked="" type="checkbox"/>	<input type="checkbox"/> ChIP-seq
<input checked="" type="checkbox"/>	<input type="checkbox"/> Flow cytometry
<input checked="" type="checkbox"/>	<input type="checkbox"/> MRI-based neuroimaging